eNeuro

Research Article: New Research | Sensory and Motor Systems

Deletion of Tsc2 in Nociceptors Reduces Target Innervation, Ion Channel Expression and Sensitivity to Heat

Dan Carlin[1], Judith P. Golden[2], Amit Mogha[3], Vijay K. Samineni[2], Kelly R. Monk[3], Robert W. Gereau[2] and Valeria Cavalli[4]

[1]*Department of Neuroscience, Washington University School of Medicine, St Louis, MO 63110*

[2]*Washington University Pain Center and Department of Anesthesiology, Washington University School of Medicine, St Louis, MO 63110*

[3]*Department of Developmental Biology, Washington University School of Medicine, St Louis, MO 63110*

[4]*Department of Neuroscience, Hope Center for Neurological Disorders and Center for Regenerative Medicine, Washington University School of Medicine, St Louis, MO 63110*

DOI: 10.1523/ENEURO.0436-17.2018

Received: 13 December 2017

Revised: 13 April 2018

Accepted: 16 April 2018

Published: 25 April 2018

Author contributions: All authors designed research as well as edited and approved the manuscript; D.C. performed histology, analyzed the data and wrote the paper; J.P.G. and V.K.S. performed and analyzed behavior experiments; A.M. performed electron microscopy.

Funding: NIH
DE022000
NS099603
NS42595

Funding: Mc Donnell Center for Cellular Neurobiology

The authors declare no competing financial interests.

NIH grants DE022000 (V.C.), NS099603 (V.C.) and NS42595 (R.W.G); McDonnell Center for Cellular Neurobiology at Washington University School of Medicine (K.R.M.).

Correspondence should be addressed to: Valeria Cavalli, Department of Neuroscience, Washington University School of Medicine, McDonnell Science 922, St. Louis, MO 63110. E-mail: cavalli@wustl.edu

Cite as: eNeuro 2018; 10.1523/ENEURO.0436-17.2018

Manuscript Title (50 word maximum): Deletion of Tsc2 in nociceptors reduces target innervation, ion channel expression and sensitivity to heat

Abbreviated Title (50 character maximum): Tsc2 deletion alters sensory behavior

Author names and affiliations: Dan Carlin, Department of Neuroscience, Washington University School of Medicine, St Louis, MO 63110; Judith P. Golden, Washington University Pain Center and Department of Anesthesiology, Washington University School of Medicine, St Louis, MO 63110; Amit Mogha, Department of Developmental Biology, Washington University School of Medicine, St Louis, MO 63110; Vijay K. Samineni, Washington University Pain Center and Department of Anesthesiology, Washington University School of Medicine, St Louis, MO 63110; Kelly R. Monk, Department of Developmental Biology, Washington University School of Medicine, St Louis, MO 63110*; Robert W. Gereau IV, Washington University Pain Center and Department of Anesthesiology, Washington University School of Medicine, St Louis, MO 63110; Valeria Cavalli, Department of Neuroscience, Hope Center for Neurological Disorders and Center for Regenerative Medicine, Washington University School of Medicine, St Louis, MO 63110

*Present address: Vollum Institute, Oregon Health & Science University, Portland, OR 97221

Author contributions: All authors designed research as well as edited and approved the manuscript; D.C. performed histology, analyzed the data and wrote the paper; J.P.G. and V.K.S. performed and analyzed behavior experiments; A.M. performed electron microscopy.

Correspondence should be addressed to: Valeria Cavalli, cavalli@wustl.edu, Department of Neuroscience, Washington University School of Medicine, McDonnell Science 922, St. Louis, MO 63110.

Number of Figures: 8
Number of Tables: 3
Number of Multimedia: 0

Number of words for Abstract: 225
Number of words for Significance Statement: 119
Number of words for Introduction: 746
Number of words for Discussion: 1680

Acknowledgements: We would like to thank the National Institutes of Health (NIH) grants DE022000 (V.C), NS099603 (V.C.) and NS42595 (R.W.G) as well as McDonnell Center for Cellular and Molecular Neurobiology (K.R.M). We would also like to thank the Genome Technology Access Center, Flow Cytometry Core and Center for Cellular Imaging facilities at Washington University. We would like to acknowledge Eric Ewan, Wolfgang Pita-Thomas, Marcus Mahar, Oshri Avraham and Guoyan Zhao for helpful discussions during manuscript preparation as well as Douglas Larson, Kathy Leahy, Breanne Harty and Dennis Oakley for technical assistance.

Conflict of Interest: The authors declare no competing financial interests.

Funding sources: NIH grants DE022000 (V.C.), NS099603 (V.C.) and NS42595 (R.W.G); McDonnell Center for Cellular Neurobiology at Washington University School of Medicine (K.R.M.).

Abstract

The mechanistic Target of Rapamycin Complex 1 (mTORC1) is known to regulate cellular growth pathways, and its genetic activation is sufficient to enhance regenerative axon growth following injury to the central or peripheral nervous systems. However, excess mTORC1 activation may promote innervation defects, and mTORC1 activity mediates injury-induced hypersensitivity, reducing enthusiasm for the pathway as a therapeutic target. While mTORC1 activity is required for full expression of some pain modalities, the effects of pathway activation on nociceptor phenotypes and sensory behaviors are currently unknown. To address this, we genetically activated mTORC1 in mouse peripheral sensory neurons by conditional deletion of its negative regulator Tuberous sclerosis 2 (Tsc2). Consistent with the well-known role of mTORC1 in regulating cell size, soma size and axon diameter of C-nociceptors were increased in Tsc2-deleted mice. Glabrous skin and spinal cord innervation by C-fiber neurons were also disrupted. Transcriptional profiling of nociceptors enriched by fluorescence-associated cell sorting (FACS) revealed downregulation of multiple classes of ion channels as well as reduced expression of markers for peptidergic nociceptors in Tsc2-deleted mice. In addition to these changes in innervation and gene expression, Tsc2-deleted mice exhibited reduced noxious heat sensitivity and decreased injury-induced cold hypersensitivity, but normal baseline sensitivity to cold and mechanical stimuli. Together, these data show that excess mTORC1 activity in sensory neurons produces changes in gene expression, neuron morphology and sensory behavior.

Significance Statement

mTORC1 activation promotes regeneration of injured peripheral axons, however it may have a negative effect on target innervation as well as alter normal sensory function and injury-induced pain. Acute and chronic mTORC1 inhibition may have different effects on sensory behavior. For the mTORC1 pathway to be considered as a therapeutic target to promote nerve regeneration, it is necessary to gain an understanding of the effects of chronic pathway activation on nociceptors and sensory behavior. We show that constitutive mTORC1 activation in nociceptors via conditional deletion of its negative regulator Tsc2 results in anomalies in cell morphology and gene expression that may underlie the decrease in noxious heat sensitivity and the attenuated nerve injury-induced cold hypersensitivity observed in Tsc2-deleted mice.

Introduction

The mechanistic Target of Rapamycin Complex 1 (mTORC1) is a potent regulator of cellular growth affecting downstream processes such as protein translation, autophagy, and cellular metabolism (Saxton & Sabatini, 2017). mTORC1 activation has been shown to promote extensive axon regeneration following traumatic injury in both the permissive peripheral and the restrictive central nervous system environments (Abe et al., 2010; K. Liu et al., 2010; Park et al., 2008). Optimal functional recovery after nerve injury requires therapeutic interventions that mediate efficient target re-innervation and minimize injury-induced neuropathic pain. Increased mTORC1 activity can result in defects in target innervation. For instance, mice with mutations in the negative mTORC1 regulator Tuberous sclerosis 2 (Tsc2) exhibit inappropriately targeted retinogeniculate projections or reduced innervation of glabrous skin (Abe et al., 2010; Nie et al., 2010). However, the functional consequences of this disrupted sensory target innervation are unknown.

Studies using local, systemic or intrathecal administration of mTORC1 inhibitors have shown that attenuation of mTORC1 signaling decreases inflammation- or nerve injury-induced pain and bone cancer pain (Geranton et al., 2009; Jiang et al., 2016; Jimenez-Diaz et al., 2008; Liang et al., 2013; Lutz et al., 2015; Obara et al., 2011; Price et al., 2007). A number of studies have also shown that acute local or systemic administration of mTORC1 inhibitor does not alter sensory thresholds in naïve mice or rats (Geranton et al., 2009; Jimenez-Diaz et al., 2008; Obara et al., 2011). Interestingly, chronic inhibition of mTORC1 results in mechanical allodynia in naïve mice by a mechanism that involves feedback activation of ERK signaling in sensory neurons (Melemedjian et al., 2013). These studies indicate that mTORC1 signaling modulates pain behavior in both naïve animals and in the context of injury. However, pharmacological mTORC1 inhibition may also have effects on non-neuronal cells that can impact pain behavior in addition to potentially attenuating mTORC1 signaling in central nervous system regions involved in pain transmission including spinal dorsal horn neurons and cortical neurons (Asante

et al., 2010; Beirowski et al., 2017; Geranton et al., 2009; Kwon et al., 2017; Obara et al., 2011). As such, the specific role of the pathway in peripheral sensory neurons is less clear.

In peripheral sensory axons, an active phosphorylated form of mTORC1 has been shown to co-localize predominantly with markers of A-fiber axons, but was also shown to be expressed in a small percentage of C-fiber axons in both the skin and the dorsal root (Geranton et al., 2009; Jimenez-Diaz et al., 2008; Obara et al., 2011). However, mTOR protein is expressed in the soma of both classes of neurons in dorsal root ganglia (DRG) (Xu et al., 2010), suggesting that mTORC1 may have functions that are specific to cell type and/or subcellular localization. Local protein synthesis in sensory axons is required for both primary and secondary hyperalgesia (Obara et al., 2012), and mTORC1 signaling is a potent activator of protein translation in sensory axons (Cho et al., 2014; Khoutorsky & Price, 2018; Terenzio et al., 2018). mTORC1 signaling has also been shown to mediate protein translation in sensory neurons in response to some pain-inducing stimuli (Melemedjian et al., 2010). While these studies have shown a requirement for mTORC1 in mediating pain responses, little is known about the consequences of excess mTORC1 activation. Mice with a genetic deletion of Eukaryotic initiation factor 4E-binding protein 1 (4EBP1), a negative regulator of protein translation that is directly inhibited by mTORC1 activity, exhibit mechanical hypersensitivity, which is reported to be spinally mediated. However, 4EBP1 was deleted in all cells thereby precluding specific analysis of peripheral sensory neurons function (Khoutorsky et al., 2015). As such, the response of sensory neurons to excess mTORC1 signaling remains to be elucidated.

In the present study, we investigated the consequences of activation of mTORC1 in sensory neurons on target innervation and sensory behavior by employing a genetic approach to delete its negative regulator Tsc2 using the sensory neuron-specific Nav1.8-Cre mouse. This strategy results in Cre expression predominantly in C-nociceptors, but also in a subpopulation of sensory neurons with myelinated axons (Agarwal et al., 2004; Shields et al., 2012). In the resulting Nav-Tsc2 mice, nociceptors displayed impaired peripheral and central target

innervation as well as a disruption in nociceptor phenotype and sensory behavior-related gene expression. Naive Tsc2-deleted mice showed reduced sensitivity to noxious heat but unchanged cold and mechanical sensitivity compared to control mice. Interestingly, Tsc2-deleted mice exhibited decreased nerve injury-induced cold hypersensitivity, however it is possible that deficiencies in innervation and gene expression may account for this phenotype.

Materials and Methods

Animals

Tsc2$^{fl/fl}$ (floxed allele; RRID:MGI:3712786; Hernandez et al., 2007), *Tsc2*$^{null/+}$ (targeted null allele; RRID:MGI:2174787; Onda et al., 1999), *Nav1.8*$^{Cre/+}$ (MGI:3042874; Agarwal et al., 2004), and *Rosa26-ZsGreen* (RRID:IMSR_JAX:007906; Madisen et al., 2010) mice were described previously. To generate experimental animals, *Nav1.8*$^{Cre/+}$*; Tsc2*$^{null/+}$ mice were crossed with *Tsc2*$^{fl/fl}$ mice. *Nav1.8*$^{Cre/+}$*; Tsc2*$^{null/fl}$ mice are referred to as Nav-Tsc2 mice. Littermate animals with genotypes *Tsc2*$^{fl/+}$, *Tsc2*$^{null/fl}$, and *Nav1.8*$^{Cre/+}$*; Tsc2*$^{fl/+}$ were used as controls as they showed no phenotypic differences from each other. For experiments using the *Rosa26-ZsGreen* reporter, control; Rosa-GFP refers specifically to *Nav1.8*$^{Cre/+}$*; Tsc2*$^{fl/+}$; *Rosa26-ZsGreen*$^{GFP/+}$ while Nav-Tsc2; Rosa-GFP refers to *Nav1.8*$^{Cre/+}$*; Tsc2*$^{fl/null}$; *Rosa26-ZsGreen*$^{GFP/+}$. Genotype was determined by PCR at weaning. Male and female mice aged 7 to 18 weeks were used for experiments unless noted otherwise. All animal procedures were performed in accordance with the [Author University] animal care committee's regulations.

Western blotting

Adult L4 DRG were dissected into cell lysis buffer (Cell Signaling) with protease and phosphatase inhibitors (Roche Applied Sciences) and manually homogenized. Protein concentration was determined by DC protein assay (Bio-Rad Laboratories) against bovine serum albumin standards. 10 μg total protein was loaded onto 10% polyacrylamide gels. Membranes were blotted with antibodies directed against the following proteins: α-tubulin (1:20,000; Abcam Cat# ab18251, RRID:AB_2210057), S6 kinase (1:1,000; Cell Signaling Technology Cat# 2708, RRID:AB_390722), phospho-S6 kinase T389 (1:750; Cell Signaling Technology Cat# 9234, RRID:AB_2269803), Tsc2 (1:1,000; Cell Signaling Technology Cat#

4308), rabbit IgG conjugated to horseradish peroxidase (1:10,000; Thermo Fisher Cat# 656120). Initially blots were probed for Tsc2 and phospho-S6 kinase, then membranes were stripped in 60 mM Tris-HCl, 2% sodium dodecyl sulfonate, pH 6.8 at 50°C for 30 minutes, washed extensively, and probed in succession for S6 kinase and α-tubulin. Blots were developed with SuperSignal West Dura (ThermoFisher) and imaged with a ChemiDoc MP imaging system (Bio-Rad Laboratories).

Immunohistochemistry

Isolated footpads were fixed by immersion in 2% paraformaldehyde, 15% saturated picric acid in phosphate-buffered saline (PBS). Spinal cord and dorsal root ganglia (DRG) were fixed via transcardial perfusion with PBS followed by 4% paraformaldehyde, isolated and immersed in 4% paraformaldehyde. Following several washes, tissue was cryoprotected in 30% sucrose in PBS and sectioned using a cryostat set to cut 18 µm, 20 µm or 30 µm sections for DRG, spinal cord and footpad, respectively.

Immunostaining was performed as follows. Following brief post-fix in 4% paraformaldehyde and several washes in PBS with 0.1% Triton X-100 (PBSTx), sections were blocked using 5% donkey serum dissolved in PBSTx. Subsequently, sections were incubated overnight at 4°C in the following primary antibodies diluted in blocking reagent: chicken anti-βIII tubulin (1:500 for footpad; Abcam Cat# ab107216, RRID:AB_10899689), rabbit anti-βIII tubulin (1:500 for spinal cord, DRG; BioLegend Cat# 802001, RRID:AB_291637), goat anti-CGRP (1:400; Bio-Rad / AbD Serotec Cat# 1720-9007, RRID:AB_2290729), rabbit anti-TrkA (1:300; Millipore Cat# 06-574, RRID:AB_310180), guinea pig anti-Substance P (1: 250; Abcam Cat# ab10353, RRID:AB_297089). *Griffonia simplicifolia* Isolectin B4 (IB4) directly conjugated to Alexa Fluor 488 or Alexa Fluor 594 (1:250; Thermo Fisher Cat# I21411 and I21413) was incubated with primary antibodies. Mouse anti-Neurofilament 200 antibody (NF200; Sigma-

Aldrich Cat# MAB5266) was directly conjugated to Alexa Fluor 488 or Alexa Fluor 594 using Apex labeling kit (Thermo Fisher) and incubated with primary antibodies at 1:200 dilution. Tissue was washed several times with PBSTx, incubated with fluorescent-conjugated secondary antibodies (1:500; Thermo Fisher Scientific) and DAPI (1:1,000) diluted in blocking reagent, washed, and mounted in ProLong Gold antifade mountant (Thermo Fisher Scientific). Images were taken with a Nikon A1R confocal or TE-2000E compound microscope and analyzed in ImageJ or FIJI (NIH).

TMP histochemistry

Following two washes with 40 mM Trizma-Maleate (TM) buffer, pH 5.6, adult L4 DRG or spinal cord sections were washed with TM buffer containing 8% (w/v) sucrose. Samples were then incubated at 37°C for two hours in TM buffer containing 8% sucrose, 6 mM thiamine monophosphate chloride and 2.4 mM lead nitrate. Samples were washed once with 2% acetic acid for one minute, then washed three times with TM buffer and developed for 10 seconds with an aqueous solution of 1% sodium sulfide. The reaction was quenched with TM buffer. Samples were mounted in ProLong Gold mountant (Thermo Fisher) and imaged by differential interference contrast (DIC) microscopy. Five sections per animal separated by ≥54 µm (DRG) or ≥180 µm (spinal cord) were analyzed.

Electron microscopy

Sciatic nerves from adult (8-18 weeks old) and postnatal day 29 (P29) animals were isolated and immersed in 2% glutaraldehyde, 4% paraformaldehyde in sodium cacodylate (Karnovsky's fixative) overnight at 4^{o}C. Nerves were again fixed in 2% osmium tetroxide in sodium cacodylate for 1 hour and then treated with gradually increasing concentration of ethanol (25%, 50%, 70%, 80%, 95%, 100% v/v) for 20 minutes each, followed by propylene oxide for 20 minutes. Nerves were treated with propylene oxide:EPON mix (2:1 for 1 hour and then 1:1 overnight) followed by

214 embedding in 100% EPON. Embedded nerve samples were baked at 65°C for 2-3 days.
215 Solidified samples were cut at 70 nm on an ultra-microtome. Sections were stained with 8%
216 uranyl acetate followed by Sato's lead stain before image acquisition on a Jeol (JEM-1400)
217 electron microscope. Images were recorded with an Advanced Microscopy Techniques V601
218 digital camera.
219
220 **Image analysis**
221 *DRG neuron counting*. The total number of L4 DRG neurons was quantified by counting βIII
222 tubulin-positive profiles (TuJ1). DRG neuron subtypes were counted as TuJ1-positive cells that
223 co-labeled subtype-specific markers. All positive profiles that were also DAPI-positive were
224 counted on every fourth section and the result multiplied by four to obtain total L4 counts for
225 DRG neurons and subtypes.
226 *DRG cell size*. Using the polygon tool in FIJI software, TMPase-positive and CGRP-positive
227 cells were outlined. Area measurements were recorded for up to twenty TMPase-positive or
228 CGRP-positive/NF200-negative or ten CGRP-positive/NF200-positive neurons from a random
229 region of each section and repeated until 100 TMPase-positive or CGRP-positve/NF200-
230 negative or 50 CGRP-positive/NF200-positive neurons were analyzed for each animal. Average
231 cell area for each animal was determined. In addition, the number of cells of small, medium and
232 large diameter were determined. Cells with area < 314 μm^2, corresponding to a spherical
233 diameter of < 20 μm^2, were characterized as small diameter. Cells with area 315-706 μm^2,
234 corresponding to a spherical diameter of 20-30 μm^2, were characterized as medium diameter.
235 Cells with area > 707 μm^2, corresponding to a spherical diameter of > 30 μm^2, were
236 characterized as large diameter.
237 *Glabrous skin (footpad)*. TuJ1-positive fibers entering the epidermis were counted by focusing
238 up and down through glabrous skin sections from the two most distal footpads of the hind paw.

A stitched single plane image was then taken of the region of interest (ROI) and the length of the epidermal-dermal border was traced. Total fibers and epidermal border length of both footpads were determined for each section. Results from five sections per animal separated by ≥120 μm were averaged. Representative sections were imaged as a z-series and a max intensity projection was generated in ImageJ.

Nav-Tsc2; Rosa-GFP spinal cord. Lumbar spinal cord sections were stained for IB4 conjugated to Alexa Fluor 594 and imaged by confocal microscopy with 2X average line scans and sequential scanning using a 60X objective. To determine GFP density, GFP signal was made binary through default auto-thresholding in ImageJ. The location of IB4 labeling in the superficial dorsal horn did not appear to be altered by Tsc2 deletion. We therefore used IB4 staining as a marker for lamina II. Lamina I was defined as the region within the dorsal horn that was dorsal to IB4 labeling. Laminas I and II were outlined, and the percent GFP-positive area was determined for each. Five sections per animal separated by ≥180 μm were analyzed and averaged. The average GFP density for each sample was normalized to the percentage of GFP-positive neurons in the L4 DRG of the same animals. These values were then normalized to the mean for controls.

Sciatic nerve electron microscopy. Axon diameter measurements were made on images of 2000X magnification by averaging the lengths of two lines through the center of the axon at right angles. At least twenty Remak bundles were analyzed per animal, corresponding to >200 axons for each P29 animal and >125 axons for each adult animal.

DRG neuron dissociation and flow cytometry

L4 DRG from control; Rosa-GFP and Nav-Tsc2; Rosa-GFP mice contralateral to a sciatic nerve crush were isolated 3 days after injury in Hanks Balanced Salt Solution with 10 mM HEPES (HBSS-H). Ipsilateral DRG were not analyzed in this study. DRG were treated at 37^{o}C with consecutive applications of papain (15 U/ml) and collagenase (1.5 mg/ml) in HBSS-H. After

washes, DRG were dissociated by trituration, passed through a 70 μm cell strainer, re-suspended in PBS with 2% fetal calf serum and subjected to flow cytometry. Cells were run through an 85 μm nozzle at 45 p.s.i. on a BD FACS Aria II machine and positively sorted for GFP signal.

Quantitative PCR

For whole DRG, adult L4 DRG from control mice were isolated bilaterally, lysed, homogenized. For FACS-sorted cells, adult L1-L6 lumbar DRG from control; Rosa-GFP mice were isolated, dissociated and sorted by flow cytometry for GFP signal. For each sample, 2500 GFP-positive cells were sorted into lysis buffer from PureLink RNA Mini Kit with 5% RiboLock RNase Inhibitor (Thermo Fisher). Total RNA was extracted with PureLink RNA Mini Kit according to manufacturer's instructions (Thermo Fisher Scientific). RNA concentration was determined by NanoDrop 2000 (Thermo Fisher Scientific) for whole DRG. All samples were reverse transcribed with High Capacity cDNA Reverse Transcription Kit (Applied Biosystems). Quantitative PCR was performed with PowerUp SYBR Green master mix on 2 ng cDNA from whole DRG or cDNA from 62.5 FACS-sorted cells with a QuantStudio 6 Flex and analyzed with QuantStudio Real-Time PCR Software v1.3 (Applied Biosystems). Validated primer sequences were obtained from PrimerBank where available (Wang et al., 2012). Additional primers were designed and validated for amplification efficiency standard curve analysis. Single amplified products were noted from melting point analyses and agarose gel electrophoresis. All primer sequences are found in Table 1. ΔΔCt analysis was used to normalize target gene expression data to the geometric mean of *Ribosomal protein L13a* (*Rpl13a*) and *Gapdh* reference gene expression. Target gene expression from FACS-sorted cells was then normalized to expression from whole DRG.

RNA-seq analysis

100 L4 DRG cells were FACS-sorted for GFP into 10 μl Clontech lysis buffer with 5% RiboLock RNase Inhibitor for each sample. Three technical replicates of 100 cells each were sorted, and libraries were prepped and sequenced separately for each biological replicate. All samples were submitted to the [Genomics core facility at Author's institution] for library preparation and sequencing. Library preparation was performed using the SMARTer Ultra Low RNA kit for Illumina Sequencing (Clontech) per manufacturer's protocol. cDNA was amplified for 13 cycles and then fragmented using a Covaris E220 sonicator using peak incident power 18, duty cycle 20%, cycles/burst 50, time 120 seconds at room temperature. cDNA was blunt ended, had an A base added to the 3'ends, and then had Illumina sequencing adapters ligated to the ends. Ligated fragments were then amplified for 15 cycles using primers incorporating unique index tags. Fragments were sequenced on an Illumina HiSeq-3000 using single reads extending 50 bases. Samples were QC'd using FastQC, aligned to mm10 using STAR-align, and counted using HTseq-count. Technical replicates were collapsed in RStudio and differential expression determined using DESeq2. Adjusted p value <0.05 and log2 fold change >0.5 or <-0.5 were used as the cutoff for differential expression. Significantly regulated genes were uploaded to MetaCore for downstream analysis to determine Gene Otology (GO) processes and molecular functions that were significantly altered in Nav-Tsc2 mice.

Data deposition

RNA-seq FastQ files were deposited at the NCBI GEO database (http://www.ncbi.nlm.nih.gov) under accession number GSE112499.

Behavioral analysis

Accelerating rotarod. Mice were assessed for gross motor function using an accelerating Rotarod (Ugo Basile). Mice were trained until they were able to remain on the Rotarod (4 rpm)

for 120 seconds. One hour after training, five consecutive trials were performed on an accelerating Rotarod with 5 minutes between trials. Latency to fall was measured as the apparatus accelerated from 4 to 40 rpm over 5 minutes.

Open field activity. Locomotion was assessed using an open field (42 cm × 42 cm × 30 cm, length × width × height) equipped with a Versamax Animal Activity Monitoring System (AccuScan Instruments). Before testing, mice were habituated to the room in their home cages for at least 1 hour. Mice were then placed in the open field during individual trials and allowed to freely explore after the experimenter exited the room. The horizontal activity, distance traveled and time moving during the 1 hour trial were determined by the Versamax software.

Pole climb down. The Pole Test was used to evaluate performance in a complex motor task. Mice are placed on a vertical metal pole that is 49 cm in height and 0.9 cm in diameter with the head of the mouse oriented upward. The time required for the mouse to turn around such that the mouse's head is oriented downward and the hind limbs are straddling the pole is recorded. In addition, the time required for the mouse to climb down to the base of the pole is recorded.

von Frey test. Varying diameter von Frey monofilaments (Stoelting, Chicago, IL) were pressed against the plantar surface of the hind paw until the filament bent. The force applied to the hind paw is dependent on the diameter of the filament. The up/down method described by Chaplan was used to determine the mechanical withdrawal threshold (Chaplan et al., 1994). Three trials were performed on each paw. The three trials were averaged to obtain the withdrawal threshold for each paw.

Cold plantar test. Mice were tested for cold sensitivity in a manner described previously (Brenner et al., 2012). Briefly, mice were acclimated on a glass plate. Crushed dry ice pellet was pressed against the glass underneath the hindpaw. Withdrawal latency was measured, with withdrawal defined as any action to move the paw vertically or horizontally away from the cold

glass. An interval of 7 minutes was allowed between paws and 15 minutes between trials. The average latency times for 2 trials from both hindpaws were averaged for each mouse.

Acetone test. Sensitivity to a cold stimulus was measured using the acetone test. One drop of acetone was applied to the plantar surface of the hind paw using a 1 ml syringe. Mice were observed for 5 minutes after each acetone application. The amount of time spent in spontaneous pain behavior was recorded. Spontaneous pain behavior was defined as shaking, flinching, or licking of the paw as well as holding the paw in an elevated position. Five trials were performed on each hind paw, and the response times for each of the five trials were summed to determine the response time for each paw.

Hargreaves test. The thermal threshold was determined by measuring the withdrawal latency to a radiant heat source (ITTC Instruments) applied to the plantar surface of the hindpaw in three separate trials for each hindpaw with a 15 min interval between trials. The withdrawal threshold was determined by averaging the withdrawal latency obtained in each of the three trials. The thermal threshold was determined at an active intensity of 18 (AI18).

Chronic constriction injury. Under 2.5% isoflurane anesthesia, the sciatic nerve was loosely ligated with 6-0 chromic gut sutures. Two ligatures separated by 3 to 5 mm were placed around the sciatic nerve. The acetone test was performed prior to surgery and at specified times after surgery on contralateral and ipsilateral hind paws.

Statistical analysis

Experimenters performing surgery, behavioral observations or image analysis were blinded to genotype. Statistically significant differences were determined by two-tailed unpaired t test, two-way RM ANOVA, or Sidak's multiple comparison test using Graphpad Prism software. F and p values are reported in text for ANOVA results while only p values are reported for t tests. Sidak's multiple comparison test was used on individual data points for figures where two-way

ANOVA was reported in text. All statistical data is included in Table 2. Statistical significance was defined by $p<0.05$.

Results

Tsc2 deletion increases cell body and axon diameters of C-fiber neurons

Previous studies have analyzed the requirement of mTORC1 for full expression of pain states primarily using pharmacological approaches to inhibit mTORC1 signaling (Ferrari et al., 2013; Geranton et al., 2009; Jimenez-Diaz et al., 2008; Melemedjian et al., 2013; Obara et al., 2015; Obara et al., 2011). However, the effect of chronic mTORC1 activation in peripheral neurons on sensory behavior has not been determined. To analyze the effect of chronic mTORC1 activation in peripheral sensory neurons, we generated mice with Tsc2 deletion in a subset of dorsal root ganglia (DRG) neurons, those expressing the voltage-gated sodium channel Nav1.8, which we designate as Nav-Tsc2 mice. Cre-mediated recombination occurs in these mice after embryonic day 17.5, and in a population that comprises greater than 90% of nociceptors and ~40% of myelinated DRG neurons. (Agarwal et al., 2004; Shields et al., 2012). Animals with genotypes $Tsc2^{fl/+}$, $Tsc2^{null/fl}$ and $Nav1.8^{Cre/+}; Tsc2^{fl/+}$ were pooled as a control group as they did not exhibit phenotypic differences from each other. Phosphorylation of p70 S6 kinase at threonine 389, a direct target of mTORC1 kinase (Isotani et al., 1999), was increased in L4 DRG of adult Nav-Tsc2 mice compared to controls (Fig. 1A), confirming mTORC1 activity was increased as a result of Tsc2 deletion in Nav1.8-positive DRG neurons. Residual Tsc2 protein expression in Nav-Tsc2 DRG was likely due to non-neuronal and Nav1.8-negative neuronal contributions.

As the Tsc2/mTORC1 signaling axis affects cellular metabolism by regulation of numerous growth-related processes (Saxton & Sabatini, 2017), we analyzed nociceptor cell size to validate that Tsc2 deletion has functional consequences for those neurons. Thiamine monophosphatase (TMPase) is a marker predominantly for nonpeptidergic neurons and is known to co-localize extensively with IB4 in DRG neurons (Zylka et al., 2008). We observed a 56% increase in the average cell area of TMPase-positive nonpeptidergic L4 DRG neurons from Nav-Tsc2 mice compared with control mice ($p<0.0001$; Fig. 1B-C,F). This increase in average

cell size was accompanied by a shift in the distribution of small, medium, and large diameter nonpeptidergic neurons. In control animals, TMPase-positive neurons were predominantly small diameter with some medium and no large diameter cells. In Nav-Tsc2 mice, some small diameter neurons were present, however most neurons were medium diameter with some large diameter neurons as well (Table 3; for cell size categories see Materials and Methods). Therefore, Tsc2 deletion increases cell size of nonpeptidergic nociceptors.

Similarly, we analyzed the cell size of peptidergic nociceptors that are CGRP-positive. This population is heterogeneous in cell size as it is comprised of both A- and C-nociceptors, which we distinguished by the presence or absence of NF200 expression, respectively. CGRP-positive neurons exhibited decreased intensity of immunostaining in Nav-Tsc2 mice, but neurons were still identifiable. The average cell area of NF200-negative peptidergic C-nociceptors in Nav-Tsc2 was increased by 60% compared to neurons from control mice ($p<0.0001$; Fig. 1D-F, arrows). Additionally, these neurons exhibited a remarkably similar shift in size distribution as nonpeptidergic nociceptors whereby the percentage of medium and large diameter neurons was increased in Nav-Tsc2 mice compared with control mice (Table 3), suggesting both classes of C-nociceptors are susceptible to metabolic anomalies as a result of Tsc2 deletion. Interestingly, we did not observe a change in the average size of peptidergic A-nociceptors (CGRP, NF200 double positive) nor in the distribution of cell sizes among this population ($p=0.4803$; Fig. 1D-F, Table 3), suggesting that Tsc2 deletion may have a limited effect on the regulation of soma size and/or cellular metabolism of these cells. Notably, Nav1.8-Cre is known to be expressed in >90% of CGRP-positive neurons, and is not restricted to C-nociceptors (Shields et al., 2012). The increased cell size of C-nociceptors in DRG from Nav-Tsc2 mice validates that Tsc2 deletion in these cells has functional consequences that are consistent with constitutive mTORC1 activation.

As cell size of C-fiber neurons was increased in Nav-Tsc2 mice, we investigated whether axon diameter was also affected. Axon diameter affects conduction velocity and alterations may

influence behavioral responses to sensory stimuli. Both nonpeptidergic and peptidergic C-fiber axons are unmyelinated and associate with Remak Schwann cells in bundles within peripheral nerves (Murinson et al., 2005). To determine if axon diameter of C-fiber neurons was affected by Tsc2 deletion, we analyzed the diameter of axons in Remak bundles of the sciatic nerve by transmission electron microscopy. The average diameter of Remak-bundled axons of adult Nav-Tsc2 mice was increased by 38% compared to controls ($p=0.0047$; Fig. 2A-B), showing that both axon and cell body size are affected by Tsc2 deletion. Generally, axons greater than one micron in diameter become myelinated during early postnatal development, while axons less than one micron in diameter are sorted into Remak bundles. However, in adult Nav-Tsc2 mice we noted a significant increase in Remak-bundled axons greater than one micron in diameter compared to controls ($p=0.0055$; Fig. 2A,C). In addition, we noted a decrease in the number of axons per Remak bundle in Nav-Tsc2 mice ($p=0.0371$; Fig. 2A,D), suggesting that axon diameter may affect Remak bundle organization.

Peripheral axons are radially sorted during the first weeks of postnatal life in mouse to associate with myelinating Schwann cells (>1 micron axon diameter) or with Remak Schwann cells (<1 micron axon diameter). To determine whether the increased axon diameter in Nav-Tsc2 mice is the result of disrupted radial sorting or excess neuronal growth post-sorting, we analyzed sciatic nerves from control and Nav-Tsc2 mice at 29 days postnatal (P29), after completion of radial sorting (Feltri et al., 2016). At P29, average axon diameter was already increased in Nav-Tsc2 mice compared to control mice ($p=0.0442$; Fig. 2A-B). However, while control mice showed no age-dependent increase in average axon diameter of unmyelinated axons, average axon diameter of Nav-Tsc2 mice increased from P29 to adult (control: $p=0.318$; Nav-Tsc2 $p=0.0258$; Fig. 2A-B). Despite the increase in average axon diameter of Nav-Tsc2 mice at P29, the percentage of bundled axons greater than one micron in diameter was not affected ($p=0.2076$; Fig. 2A,C). Consistently, there was no change in the number of axons per bundle at P29 in Nav-Tsc2 mice compared to control mice ($p=0.0747$; Fig. 2D). However, there

447 was a statistically significant age-related decline in the number of axons per bundle in sciatic
448 nerves from Nav-Tsc2 mice that was not seen in controls (control: p=0.5018; Nav-Tsc2
449 p=0.0202; Fig. 2A,D). Together these data are consistent with the notion that axons are sorted
450 properly by size during early postnatal development, and axonal hypertrophy after sorting
451 reduces the number of axons per bundle. This may be due to Remak Schwann cell hyperplasia
452 or Remak fragmentation or elaboration of Schwann cell processes, as has recently been
453 described following injury (Gomez-Sanchez et al., 2017).
454
455 **Peripheral and central target innervation are preferentially disrupted by loss of Tsc2**
456 As axon morphology was affected in Nav-Tsc2 mice and previous studies have shown that Tsc2
457 deletion mediated by Advillin-Cre reduces innervation of glabrous skin (Abe et al., 2010), we
458 analyzed C-fiber target innervation in Nav-Tsc2 mice. To determine if skin innervation is
459 disrupted in Nav-Tsc2 mice, we performed immunohistochemistry for the pan-neuronal marker
460 βIII-tubulin (TuJ1) to assess total intraepidermal nerve fiber (IENF) density of glabrous skin of
461 the hindpaw footpads. Similar to Advillin-Tsc2 mice, Nav-Tsc2 mice showed a significant
462 reduction of total IENF density ($p<0.0001$; Fig. 3A-C). We also observed aberrant morphology of
463 fibers similar to previously reported (Fig. 3B arrowhead; Abe et al., 2010). As Cre expression
464 occurs perinatally from the Nav1.8 transgene in contrast to embryonic day 12.5 expression of
465 Advillin-Cre (Agarwal et al., 2004; Hasegawa et al., 2007), these data suggest that mTORC1
466 activation after embryonic development is sufficient to affect peripheral target innervation.
467 The central processes of C-nociceptors project to superficial lamina of the spinal cord
468 dorsal horn. Specifically, peptidergic (CGRP-positive) C-nociceptors project to lamina I and
469 outer lamina II (II_o) while nonpeptidergic (IB4-positive) C-nociceptors project to inner lamina II
470 (II_i; Fig. 4A,C,G). To determine if DRG neuron fiber density was disrupted in the dorsal horn by
471 Tsc2 deletion, we crossed a floxed *Rosa-GFP* reporter into control (specifically, $Nav1.8^{Cre/+}$;
472 $Tsc2^{fl/+}$) and Nav-Tsc2 mice. Using IB4 as a marker of lamina II, we analyzed the percent area

occupied by GFP signal in laminas I and II. We observed a reduction in GFP-positive area in both dorsal horn lamina in Nav-Tsc2; Rosa-GFP mice compared to control; Rosa-GFP mice (lamina I: p=0.0403; lamina II: p=0.0002; Fig. 3D-F), suggesting target innervation is disrupted in both the peripheral and central branches of C-fiber neurons.

Despite the reduction in dorsal horn fiber density in Nav-Tsc2 mice, the proper targeting of each class of C-nociceptor to its appropriate superficial lamina of the lumbar spinal cord was unaffected (Fig. 4A-F). In addition to superficial lamina, CGRP-positive fibers project to deep laminae (Fig. 4A, arrows). Strong reduction of CGRP innervation to deep laminae was observed in all Nav-Tsc2 mice compared to control mice (Fig. 4A-B, arrows), however reduced expression levels of CGRP may contribute to this phenotype.

In analyzing nonpeptidergic innervation of the lumbar spinal cord, we surprisingly observed ectopic IB4 binding that presented as filamentous or axon-like labeling in the dorsal white matter of the spinal cord in all Nav-Tsc2 mice, a phenotype never seen in control animals (Fig. 4D,F). IB4 is a lectin and can potentially bind to multiple proteins. Ectopic binding may result from upregulation of a binding target in that region or from mistargeting of nonpeptidergic axons into the white matter. Thiamine monophosphatase (TMPase) is a marker for predominantly nonpeptidergic neurons that is known to co-localize extensively with IB4 in DRG and is present in DRG cell bodies as well as dorsal horn axon terminals (Bennett et al., 1998; Zylka et al., 2008). We performed TMP histochemistry on spinal cord sections to determine if ectopic IB4 binding in the spinal cord of Nav-Tsc2 mice is a result of aberrant targeting of nonpeptidergic nociceptor axons. We did not observe TMPase-positive nonpeptidergic axon terminals outside of the dorsal horn superficial laminae in Nav-Tsc2 mice (Fig. 4G-H), suggesting that targeting of nonpeptidergic axon terminals was normal in these mice. To further investigate the nature of the ectopic IB4 labeling, we crossed a floxed *Rosa-GFP* reporter into control and Nav-Tsc2 mice. GFP signal was strong in axons of control; Rosa-GFP and Nav-Tsc2; Rosa-GFP mice in both grey and white matter (Fig. 3D-E, 4I-K), consistent with GFP

499 expression driven in ~40% of myelinated DRG neurons some of which project to the white
500 matter (Shields et al., 2012). However, IB4 labeling was interspersed between GFP signal in
501 regions of the dorsal white matter, and co-localization of filamentous IB4 labeling with GFP
502 fluorescence was not seen in lateral dorsal white matter (Fig. 4I-K). We conclude that ectopic
503 IB4 labeling in spinal cord white matter of Nav-Tsc2 mice does not result from aberrant targeting
504 of nonpeptidergic axons.
505
506 **Tsc2 is required for the full expression of peptidergic markers and ion channels in**
507 **nociceptors**
508 Reduced nociceptor target innervation in Nav-Tsc2 mice could result from several possible
509 mechanisms. One such mechanism is a reduction in the number of DRG neurons that project to
510 those targets. To explore this possibility, we counted total neurons as well as presumptive
511 myelinated neurons in adult L4 DRG of control and Nav-Tsc2 mice using antibodies directed
512 against TuJ1 and NF200, respectively. Loss of Tsc2 resulted in no change in the total neuron
513 number nor in the number of NF200-positive neurons (TuJ1: p=0.081; NF200: p=0.314; Fig. 5A-
514 E).
515 To analyze the effects of Tsc2 deletion on specific nociceptor populations, we counted
516 peptidergic nociceptors in L4 DRG that are immunoreactive for Substance P (SP), CGRP, and
517 TrkA. mRNA expression of CGRP (*Calca* and *Calcb*) and TrkA (*Ntrk1*) was reduced in Nav-Tsc2
518 DRG, however SP (*Tac1*) expression was normal (Fig. 7B, Extended Data Figure 7-1). Despite
519 this differential regulation of mRNA expression, we observed similar phenotypes by
520 immunohistochemistry for all three markers. For each, we observed a decrease in the intensity
521 of immunoreactivity in DRG neurons from Nav-Tsc2 mice, however these neurons were still
522 identifiable (Fig. 1D-E, Fig. 5A-B,D-E,G-H). The number of SP neurons was reduced in Nav-
523 Tsc2 DRG compared to controls (p=0.0006; Fig. 5A-B,F). CGRP and TrkA neurons can project
524 Aδ- or C-fiber axons, which are distinguishable by NF200 expression. Reductions were noted in

the number of both NF200-negative and NF200-positive CGRP neurons as well as TrkA neurons in Nav-Tsc2 DRG compared to controls (CGRP+,NF200-: $p<0.0001$; CGRP+,NF200+: $p=0.0007$; TrkA+,NF200-: $p<0.0001$; TrkA+,NF200+: $p=0.0005$; Fig. 5D-G). While the number of peptidergic neurons may be underestimated due to decreased expression levels of these markers, these data suggest a strong reduction in phenotypic markers of peptidergic nociceptors.

As peptidergic nociceptor number was reduced and the total number of neurons was unaffected in Nav-Tsc2 mice, we predicted an expansion of other populations of DRG neurons. Consistently, we noted a 34% increase in the average number of IB4 neurons in the DRG of Nav-Tsc2 mice compared to controls ($p=0.0001$; Fig. 5J-L). Co-labeling of IB4 and NF200 was rarely observed in control animals, however to our surprise, we identified a notable population of neurons that were positive for both IB4 and NF200 in Nav-Tsc2 mice ($p=0.0037$; Fig. 5J-L arrows). The size of this novel population accounted for the loss of NF200-positive CGRP or TrkA neurons and comprises 8.6% of the total IB4 population. As we did not observe ectopic IB4 or TMP labeling in deep laminae of the dorsal horn of Nav-Tsc2 mice (Fig. 4D,H), these supernumerary IB4-positive neurons may project to lamina II_i, the normal target of IB4-positive afferents. Together, these data show a gain of IB4-positive DRG neurons at the expense of peptidergic nociceptors in Nav-Tsc2 mice.

To gain insight into the gene expression changes in DRG neurons resulting from Tsc2 deletion, we performed transcriptional profiling of neurons from control; Rosa-GFP and Nav-Tsc2; Rosa-GFP mice. L4 DRG neurons from these mice were dissociated, and GFP-positive cells were sorted by flow cytometry. Libraries were prepped from 100 GFP-positive cells and subjected to RNA-seq analysis (Fig. 6A-B). To determine the relative enrichment of nociceptors by FACS-sorting, we performed quantitative PCR (qPCR) on control whole DRG and FACS-sorted GFP-positive cells from control DRG with markers of different neuron populations as well as glial markers. *TrkA* and *Nav1.8* expression was determined to denote nociceptors, while

551 *TrkB* and *TrkC* were assayed for mechanoreceptors and proprioceptors, respectively (Usoskin
552 et al., 2015). *Periaxin* (*Prx*) and *Egr2* (*Krox20*) were assayed as glial markers (Jones et al.,
553 2007; Svaren & Meijer, 2008). We noted >3-fold increase in *TrkA* and a trend towards a 1.5-fold
554 increase in normalized levels of *Nav1.8* in FACS-sorted samples relative to whole DRG (*TrkA*:
555 p=0.0014; *Nav1.8*: p=0.0613; Fig. 6C). While we observed no change in the relative levels of
556 *TrkB*, we observed a 60% reduction in normalized levels of *TrkC* in FACS-sorted samples
557 compared to whole DRG (*TrkB*: p=0.9758; *TrkC*: p=0.002; Fig. 6C). Glial markers *Prx* and *Egr2*
558 exhibited an average ~16-fold and ~2-fold reduction in FACS-sorted samples respectively,
559 however these changes did not attain statistical significance due to high inter-sample variability
560 (*Prx*: p=0.178; *Egr2*: p=0.5834; Fig. 6C). Together this suggests that our FACS-sorted samples
561 are highly enriched for nociceptors, with some glial and other neuron contamination.

562 We then performed Gene Ontology (GO) analysis on the genes differentially expressed
563 in Nav-Tsc2; Rosa-GFP compared to control; Rosa-GFP DRG (adjusted p value <0.05, log2
564 fold change >0.5 or <-0.5) and found that many of the downregulated categories of GO
565 processes and molecular functions with the highest statistical significance relate to ion channel
566 expression (Fig. 6D). To understand transcriptional shifts in ion channel expression in Nav-Tsc2
567 mice (Fig. 7A), we utilized the gene lists from a previously published study that also used FACS-
568 sorting of DRG neurons expressing a fluorescent reporter in an Nav1.8-Cre dependent manner
569 (Chiu et al., 2014). This study identified genes in a number of different categories that are
570 expressed in DRG neurons. We noted reduced expression of *Calca* (*CGRPa*) and *Ntrk1* (*TrkA*),
571 consistent with our cell counting results, as well as several sensory behavior mediators of itch
572 including *Nppb* and *Mrgpra3* (Fig. 7B). In DRG from Nav-Tsc2; Rosa-GFP mice, there was a
573 preference towards downregulation of a number of sodium, potassium and calcium channels as
574 well as G protein-coupled receptors (Fig. 7C-E,I). Other categories, including chloride, Trp and
575 ligand-gated ion channels as well as transcription factors, showed a more random distribution of
576 upregulated and downregulated genes in DRG from Nav-Tsc2; Rosa-GFP mice compared to

control; Rosa-GFP (Fig. 7F-H,J). Differential expression data for individual genes can be found in the Extended Data Figure 7-1.

The previous report of DRG transcriptional profiling identified the 40 most enriched genes in IB4-positive and IB4-negative subgroups of Nav1.8-positive neurons (Chiu et al., 2014). As Nav-Tsc2 mice have an increase in the number IB4-positive neurons at the expense of IB4-negative ones, we analyzed the enriched gene sets from Chiu et al. to determine if these genes are enriched in DRG from Nav-Tsc2 mice. Although we noted an increase in the number of IB4-positive neurons in DRG from Nav-Tsc2 mice (Fig. 5J-L), the expression of most genes previously shown to be enriched in IB4-positive neurons was unchanged in Nav-Tsc2 mice, and an equal number of genes were up- and downregulated (Fig. 7K). In contrast, we observed a reduction in the expression of the peptidergic markers SP, CGRP and TrkA by immunohistochemistry (Fig 5), and also noted a strong reduction in the expression of genes enriched in the IB4-negative group. Of the 38 IB4-negative enriched genes found in our dataset, 28 were downregulated while only one was upregulated in DRG from Nav-Tsc2 mice (Fig. 7L). Together, this suggests notable deficits in peptidergic nociceptors in Nav-Tsc2 mice that may affect their function.

Nav-Tsc2 mice have reduced sensitivity to noxious heat and decreased nerve injury-induced cold hypersensitivity

As nociceptors from Nav-Tsc2 mice showed altered target innervation and altered expression of some genes related to nociceptor phenotypes and sensory behaviors, we evaluated sensory behavior in these mice including sensitivity to heat, cold and mechanical stimuli. As a result of reduced expression of markers of peptidergic nociceptors, we hypothesized that Nav-Tsc2 mice might exhibit a phenotype similar to mice in which CGRP neurons are ablated (i.e. with reduced sensitivity to heat and cold hypersensitivity) (McCoy et al., 2013). We analyzed male and female mice independently due to gender-dependent differences in sensory thresholds. Using the von

603 Frey test for mechanical sensitivity, we observed no differences in the withdrawal threshold
604 between control and Nav-Tsc2 mice (female: p=0.2513; male p=0.462; Fig. 8A). We also
605 observed no differences in response to a cold stimulus between control and Nav-Tsc2 mice in
606 the cold plantar assay or the acetone test (female: p=0.239; male p=0.2102; Fig. 8B,D-E). In
607 contrast, both male and female Nav-Tsc2 mice displayed a decrease in sensitivity to noxious
608 heat compared to control animals (female: p=0.0046; male p=0.0337; Fig. 8C), consistent with
609 our prediction. To confirm that decreased sensitivity was not due to altered sensorimotor
610 behavior, control and Nav-Tsc2 mice were subjected to a battery of tests to evaluate motor
611 function. Control and Nav-Tsc2 mice were not distinguishable in any test performed, and
612 therefore we report several representative tests. Nav-Tsc2 mice displayed a trend towards a
613 better performance on the accelerating Rotarod compared to controls (F=4.08, p=0.0518; Fig.
614 8F). Additionally, no significant differences were noted between control and Nav-Tsc2 mice in
615 open field activity (p=0.8027; Fig. 8G) or in the pole test which evaluates performance of a
616 complex motor task (F=0.0425, p=0.8376; Fig. 8H). Motor behavior of Nav-Tsc2 mice was
617 indistinguishable from controls, indicating that changes in sensory behavioral responses were
618 not due to motor impairment.

619 mTORC1 inhibition by rapamycin injection has been shown to reduce mechanical
620 hypersensitivity in chronic pain models such as spared nerve injury (Geranton et al., 2009;
621 Jimenez-Diaz et al., 2008), however similar analysis has not been performed in the context of
622 constitutive mTORC1 activation specifically in nociceptors. Due to the previously reported
623 requirement for mTORC1 activation and local protein translation for the full expression of nerve-
624 injury-induced pain behaviors (Khoutorsky & Price, 2018), we expected to see increased nerve-
625 injury-induced hypersensitivity in Nav-Tsc2 mice. To determine whether mTORC1 activation
626 affects nerve injury-induced hypersensitivity, we analyzed cold hypersensitivity induced by
627 chronic constriction injury (CCI) of the sciatic nerve. We initially measured CCI-induced
628 mechanical hypersensitivity and CCI-induced cold hypersensitivity in Nav-Tsc2 mice and control

mice using the Von Frey test and the acetone test, respectively. We observed inconsistent CCI-induced mechanical hypersensitivity in Nav-Tsc2 mice and control mice. However, both Nav-Tsc2 mice and control mice developed robust and stable cold hypersensitivity following CCI. We therefore used the acetone test as a measure of CCI-induced hypersensitivity. Cold sensitivity as measured by the acetone test was not affected at baseline in Nav-Tsc2 mice (Fig. 8D-E). While the acute phase of hypersensitivity in the first week following CCI was not affected by Tsc2 deletion, we observed a statistically significant reduction of nerve injury-induced cold hypersensitivity for females and a trend towards similar attenuation in male Nav-Tsc2 mice in the chronic phase several weeks after injury (female: $F=9.032$, $p=0.0089$; male: $F=3.403$, 0.0807; Fig. 8D-E), contrary to our prediction. These data suggest that Tsc2 deletion and consequent chronic mTORC1 activation attenuates nerve injury-induced cold hypersensitivity.

Discussion

In the present study, we analyzed the effects of Tsc2 deletion and chronic activation of mTORC1 in sensory neurons, primarily nociceptors, on peripheral and central target innervation, gene expression and sensory behavior. Consistent with the well-defined role of Tsc2 and mTORC1 in regulating cell size, we found an increase in cell soma size and axon diameter of C-fiber nociceptors in Nav-Tsc2 mice compared with nociceptors in control mice. To our surprise, we also found that Tsc2 deletion in nociceptors resulted in phenotypic changes in subpopulations of nociceptors, which manifested as a decrease in the number of peptidergic nociceptors with a concomitant increase in the number of IB4-positive neurons (presumably nonpeptidergic nociceptors). In addition, we found that deletion of Tsc2 and consequent chronic mTORC1 activation in sensory neurons resulted in decreased sensitivity to noxious heat as well as decreased nerve injury-induced cold hypersensitivity in Nav-Tsc2 mice. Together, these data show that Tsc2 functions to control target innervation and is required for full expression of nociceptor phenotypes and the expression of sensory-related genes. Disruption of Tsc2 in sensory neurons also results in abnormal sensory behavior, which may be due to the observed phenotypic changes in DRG neurons in which Tsc2 is deleted.

Cell size and axon diameter are regulated by Tsc2 in C-nociceptors

mTORC1 is a well-characterized regulator of cell size (Fingar et al., 2002). Patients with tuberous sclerosis complex have a chronic increase in mTORC1 signaling as a result of genetic disruption of Tsc1 or Tsc2. In mouse models, deletion of Tsc1 generated enlarged neuronal somata in hippocampal and cortical neurons (Meikle et al., 2007; Tavazoie et al., 2005). Consistent with these prior studies, our results show that cell size of unmyelinated peripheral sensory neurons is also increased in Tsc2-deleted mice, although we observed no effect on CGRP-positive presumptive myelinated neurons. It is possible that A-nociceptors normally have relatively high levels of an activated form of mTORC1 (Geranton et al., 2009; Jimenez-Diaz et

al., 2008; Obara et al., 2015), which may result in increased baseline activity levels that make them less sensitive to constitutive mTORC1 signaling. Alternatively, A-nociceptors may engage compensatory mechanisms following Tsc2 deletion that maintain normal levels of cellular metabolism and/or cell morphology.

Peripheral axon diameter of C-fibers was increased in addition to soma size in Nav-Tsc2 mice. A similar increase in axon diameter was also observed in corpus callosum of mice with neuron-specific Tsc1 deletion (Ercan et al., 2017). Neuron-specific Tsc1 deletion also results in hypomyelination as a result of increased connective tissue growth factor (CTGF) expression (Ercan et al., 2017; Meikle et al., 2007). Similar to hypomyelination in a mouse model, white matter defects have also been noted in tuberous sclerosis patients (Ridler et al., 2001). We did not analyze myelination in the Nav-Tsc2 mice because Tsc2 was deleted primarily in unmyelinated C-nociceptors and only a subset of myelinated neurons. We did however observe disorganized bundles of C-fiber axons associated with Remak Schwann cells. We observed fewer axons per Remak bundle in adult but not in P29 Nav-Tsc2 animals when sorting axons by size is completed. It is possible that as Nav-Tsc2 axons continue to grow inside bundles after the completion of radial sorting, the Remak Schwann cell undergoes hypertrophy to compensate for increased axon volume or extrudes axons to maintain its size. Alternatively, Remak Schwann cells may undergo fragmentation or elaboration of processes, which was recently reported in injured nerves (Gomez-Sanchez et al., 2017). Remak Schwann cell hyperplasia may facilitate increased numbers of Remak Schwann cells to re-bundle extruded axons, or if axons are larger than one micron in diameter they may become wrapped by myelinating Schwann cells. Future studies examining neuron-glia interactions in older mice with sensory neuron deletion of Tsc2 are required to determine if this phenotype is progressive or stably maintained.

Tsc2 deletion disrupts nociceptor target innervation, gene expression and sensory behavior

Previous studies using pharmacological approaches have found that inhibition of mTORC1 signaling in the periphery, spinal cord or brain can attenuate bone cancer pain as well as inflammation- and nerve injury-induced pain (Asante et al., 2010; Ferrari et al., 2013; Geranton et al., 2009; Jiang et al., 2016; Jimenez-Diaz et al., 2008; Kwon et al., 2017; Liang et al., 2013; Obara et al., 2011; Price et al., 2007). These previous reports indicate that mTORC1 signaling at a peripheral and/or central locus within the pain transmission pathway is required for the full expression of these pain states. Conversely, 4EBP1 knockout mice, which would mimic global constitutive activation of mTORC1 on a single downstream effector, exhibit mechanical hypersensitivity (Khoutorsky et al., 2015). We thereby hypothesized that chronic mTORC1 activation would promote hypersensitivity to sensory stimuli. On the contrary, we found that chronic activation of mTORC1 in sensory neurons results in decreased sensitivity to noxious heat in naïve mice and decreased nerve injury-induced cold hypersensitivity, suggesting that chronic activation of mTORC1 in nociceptors may decrease pain.

There are a number of important differences between the current study and previous studies that have employed a pharmacological or global knockout approach to modulate mTORC1 signaling. First, we used a genetic strategy to specifically activate mTORC1 in sensory neurons, primarily nociceptors. The use of mTORC1 inhibitors in previous studies likely influences multiple cell types which may impact sensory behavior including primary sensory neurons, spinal neurons and cortical neurons as well as of a number of non-neuronal cells that may influence sensation including immune cells, Schwann cells, DRG satellite glia, and CNS glial cells (Asante et al., 2010; Beirowski et al., 2017; Ferrari et al., 2013; Geranton et al., 2009; Kwon et al., 2017; Nicks et al., 2014). Inhibition of mTORC1 signaling in all or some of these diverse cell types simultaneously is likely to have a complex effect on sensory behavior. In addition to nociceptor specificity, our study chronically activated mTORC1 signaling. Most

718 previous studies using mTORC1 inhibitors administered non-continuously and during a limited
719 timeframe have found that mTORC1 inhibitors attenuate pain. There is evidence that chronic
720 modulation of mTORC1 signaling may produce different effects compared with acute
721 modulation. For example, chronic treatment of human patients or mice with mTORC1 inhibitors
722 produces an increased incidence of pain (Budde et al., 2011; McCormack et al., 2011;
723 Melemedjian et al., 2013). We report an attenuation in pain as a result of chronic mTORC1
724 activation in sensory neurons that express Nav1.8.

725 In Nav-Tsc2 mice, we observed disruptions in nociceptor soma and axon size, target
726 innervation and gene expression including sensory behavior-related genes. Any or all of these
727 changes may contribute to the attenuation of pain in Nav-Tsc2 mice. Cre expression in Nav1.8-
728 Cre transgenic mice is initiated at embryonic day 17.5 (Agarwal et al., 2004), however cell fate
729 determination of peptidergic and nonpeptidergic nociceptors is not complete until after the third
730 postnatal week in mice (Molliver et al., 1997). Therefore, the sensory behavior changes
731 observed in Nav-Tsc2 mice may be a result of developmental abnormalities in DRG neuron
732 specification or a failure to maintain a nociceptor phenotype in maturity. Previous studies in
733 which DRG phenotype specification was altered by perturbing expression of the transcription
734 factor Runx1 in an Nav1.8-Cre dependent manner resulted in changes in DRG target
735 innervation and in sensory behavior (Abdel Samad et al., 2010; Chen et al., 2006; Yang et al.,
736 2013). Attenuated pain responses in Nav-Tsc2 mice may similarly be a result of developmental
737 anomalies. Innervation defects in Nav-Tsc2 mice may result from failure to innervate target
738 tissue or from axon retraction. For instance, long-term maintenance of increased axon diameter
739 in Nav-Tsc2 mice may pose a negative impact on axon health and morphology, which in turn
740 may cause retraction from targets. The disruptions in axon morphology found in Nav-Tsc2 mice
741 may underlie the observed sensory behavioral changes.

742 Nociceptor subpopulations have been correlated with modality-specific sensory
743 responses (Cavanaugh et al., 2009; McCoy et al., 2013). CGRP-positive neurons are required

744 for heat sensitivity, but also tonically suppress cold sensitivity (McCoy et al., 2013). Therefore,
745 the observed hyposensitivity to noxious heat in Nav-Tsc2 mice is consistent with preferential
746 disruption of CGRP neurons. Although we did not test responses to pruritogens in this study, we
747 would also predict that responses to some pruritogens may be reduced due to decreased
748 expression of *MrgprA3*, *Nppb* and *Il31ra* (Cevikbas et al., 2014; Q. Liu et al., 2009; McCoy et al.,
749 2013; Mishra & Hoon, 2013). We did not observe a change in baseline cold sensitivity in these
750 mice. Mechanical sensitivity, a modality that requires nonpeptidergic nociceptors (Cavanaugh et
751 al., 2009), was unchanged in Nav-Tsc2 mice, consistent with the comparatively normal gene
752 expression of these neurons. It is not yet clear whether changes in innervation density and gene
753 expression are related to disrupted nociceptor development or maintenance, however they likely
754 are contributors to reduced sensitivity in Nav-Tsc2 mice.

755 As mTORC1 is required for full expression of inflammatory and neuropathic pain states
756 (Lutz et al., 2015; Obara & Hunt, 2014), we predicted that constitutive activation of the pathway
757 would produce hypersensitivity in naïve mice. On the contrary, we observed normal mechanical
758 and cold thresholds and decreased sensitivity to heat in naïve Nav-Tsc2 mice as well as
759 decreased cold hypersensitivity after nerve injury. From these results, it is enticing to conclude
760 that mTORC1 activation does not promote pain, and may even reduce it. However, genetic
761 mTORC1 activation induced complex changes in nociceptors from Nav-Tsc2 mice that may
762 cooperate to generate the observed behaviors. It will be important to investigate the effects of
763 chronic mTORC1 activation on sensory behavior in mice in which mTORC1 activation is
764 initiated in adulthood using inducible Cre expression or pharmacological means. A recent study
765 found that adult deletion of Pten, a negative regulator of mTORC1 activity farther upstream than
766 Tsc2, did not alter baseline mechanical or thermal thresholds (Gallaher & Steward, 2018).
767 However, the regeneration enhancement in these mice was very modest, suggesting that Pten
768 may be a less potent regulator of the mTORC1 pathway in the peripheral nervous system than
769 Tsc2. Adult deletion of Tsc2 in sensory neurons will be required to determine if the

770 Tsc2/mTORC1 signaling axis can be activated after nerve injury to enhance regenerative axon
771 growth without stimulating pain.

772 **Figure Legends**

773 **Figure 1.** Tsc2 deletion in Nav1.8-positive neurons activates mTORC1 signaling and increases
774 soma size. (**A**) Western blot of L4 DRG from adult Nav-Tsc2 mice showed decreased
775 expression of Tsc2 and increased phosphorylation of the direct mTORC1 target S6 kinase T389
776 relative to control mice. N=8-10. kDa, kilodaltons. (**B**-**C**) TMP histochemistry of adult control and
777 Nav-Tsc2 L4 DRG. Scale bar: 50 μm. N=6. (**D**-**E**) Immunohistochemistry of adult control and
778 Nav-Tsc2 L4 DRG for CGRP and NF200. Arrows point to CGRP-positive, NF200-negative
779 neurons. N=5. (**F**) Average cell area of labeled neurons. Individual animals plotted with mean ±
780 SEM. N.S $p>0.05$, **** $p < 0.0001$.

781 **Figure 2.** C-fiber axon diameter is increased in Nav-Tsc2 mice. (**A**) Transmission electron
782 micrographs of representative transverse sections of sciatic nerve of P29 (N=5) and adult (N=6)
783 mice. Arrows point to axons greater than one micron in diameter. Scale bar: 1 μm. (**B**) Average
784 diameter of axons bundled by Remak Schwann cells. (**C**) Percentages of axons bundled by
785 Remak Schwann cells that have diameter greater that one micron. (**D**) Average number of
786 axons within individual Remak bundles. Individual animals plotted with mean ± SEM. * $p<0.05$,
787 ** $p < 0.01$.

788 **Figure 3.** Fiber innervation is reduced in both central and peripheral targets of DRG neurons in
789 Nav-Tsc2 mice. (**A**-**B**) Projection of a z-stack of hindpaw glabrous skin labeled with TuJ1.
790 Arrowhead shows aberrant fiber morphology in Nav-Tsc2 mice. Dotted line denotes epidermal-
791 dermal border. Scale bar: 50 μm. (**C**) Number of TuJ1-positive fibers crossing the epidermal-
792 dermal border were counted in control and Nav-Tsc2 mice. N=5. (**D**-**E**) Confocal micrographs of
793 Rosa-GFP reporter in control and Nav-Tsc2 lumbar spinal cord transverse sections labeled with
794 IB4. Lamina I and II used for quantification are outlined. Scale bar: 50 μm. (**F**) Normalized area
795 fraction of GFP signal in laminas I and II. N=5. Individual animals plotted with mean ± SEM. *
796 $p<0.05$. *** $p<0.001$, **** $p<0.0001$.

Figure 4. Laminar targeting of peptidergic and nonpeptidergic fibers is normal in dorsal horn of Nav-Tsc2 mice. (**A**-**F**) Control and Nav-Tsc2 lumbar spinal cord transverse sections labeled with CGRP (A,B) or IB4 (C,D) as well as merged images (E,F). Note ectopic binding of IB4 in dorsal white matter of Nav-Tsc2 mice (D,F). Arrows show deep lamina innervation by CGRP. Scale bar: 500 μm. N=7. (**G**-**H**) TMP histochemistry of control and Nav-Tsc2 lumbar spinal cord transverse sections. Scale bar: 500 μm N=11. (**I**-**K**) High magnification confocal micrographs of lumbar spinal cord transverse sections from Nav-Tsc2; Rosa-GFP mice imaged for GFP fluorescence and IB4 labeling. Note lack of co-localization in the dorsal column (DC) white matter compared to dorsal horn (DH) grey matter. Scale bar: 50 μm. N=5.

Figure 5. Peptidergic nociceptor markers are reduced in DRG from Nav-Tsc2 mice. Immunohistochemisty of adult L4 DRG transverse sections stained for SP and TuJ1 (**A**-**B**) or NF200 and CGRP (**D**-**E**), NF200 and TrkA (**G**-**H**) or NF200 and IB4 (**J**-**K**). Scale bar: 100 μm. Arrows point to neurons that co-labeled with NF200. (**C**,**F**,**G**,**L**) Total number of L4 DRG neurons labeling with markers as indicated. Individual animals plotted with mean ± SEM. N=4-6. N.S. $p>0.05$, ** $p<0.01$, *** $p<0.001$, **** $p<0.0001$.

Figure 6. Transcriptional profiling of nociceptors reveals reduction of ion channel expression in Nav-Tsc2 DRG. (**A**) Experimental design for transcriptional profiling. (**B**) After gating by forward and side scatter, FITC-positive events were purified. (**C**) qPCR comparison of normalized neuronal and glial markers from FACS-sorted cells relative to whole DRG. (**D**-**E**) Top ten Gene Ontology (GO) processes (D) and molecular functions (E) by statistical significance that were upregulated and downregulated in Nav-Tsc2 DRG as determined by p value. ** $p<0.01$.

Figure 7. Tsc2 is required for full expression of ion channels and markers of IB4-negative DRG neurons. (**A**) Model of expression changes in Nav-Tsc2 mice. (**B**-**L**) Scatterplots of normalized counts in control and Nav-Tsc2 mice for candidate genes involved in sensory behavior (B), ion channels (C-H), G protein-coupled receptors (I), transcription factors (J), and the most enriched genes in IB4-positive (K) and IB4-negative (L) neurons expressing Nav1.8-Cre (Chiu et al.,

2014). Red and blue points denote upregulated and downregulated genes, respectively, in Nav-Tsc2 DRG compared to control (adjusted $p<0.05$, log2 fold change >0.5 or <-0.5). Grey points denote no change in expression. Gene lists and values can be found in Extended Data Figure 7-1. Select genes that were highly differentially expressed in each category are highlighted. Numbers in bottom left corner of panels denote number of upregulated (red), downregulated (blue) and unchanged (black) genes analyzed. Dotted line is representative plot of y=x for reference purposes only.

Figure 8. Nav-Tsc2 mice shows normal responses to mechanical and cold stimuli but have decreased heat sensitivity and injury-induced cold hypersensitivity. (**A**-**C**) Sensory behavior analysis of control and Nav-Tsc2 mice. (A) Withdrawal threshold for control and Nav-Tsc2 male and female mice using von Frey test. N=12-13. (B) Latency to paw withdrawal from cold stimulus. N=4-11. (C) Latency to paw withdrawal in Hargreaves test. Individual animals plotted with mean ± SEM. N=9-13. (**D**-**E**) Time spent in spontaneous pain behavior as a result of acetone application to paw of uninjured (circles) or injured (triangles) hindpaw at baseline and indicated time after chronic constriction injury (CCI) for female (D) and male (E) Nav-Tsc2 mice (closed shapes) and their control littermates (open shapes). Plotted as mean ± SEM. N=8-11. BL, baseline. POD, post-operative day. (**F**-**H**) Sensorimotor battery showed no difference between control and Nav-Tsc2 mice. (F) Time to fall off an accelerating Rotarod was measured for Nav-Tsc2 mice (closed) and their control littermates (open). Data are graphed for each of five trials. N=17 (G) Open field locomotor behavior was assessed over 1 h in Nav-Tsc2 mice and their control littermates with individual data points plotted. N=23. (H) Time required to climb down a pole was measured for Nav-Tsc2 mice (closed) and their control littermates (open). Data graphed for each of two trials. N=22. Data in G-H shown as mean ± SEM. N.S. $p>0.05$, * $p<0.05$, ** $p<0.01$.

Table 1. Primer sequences used for qPCR analysis.

Table 2. Statistical table.

849 **Table 3.** Percent of small, medium, and large diameter neurons labeled with cell type-specific
850 markers. Data are presented as mean percentage ± SEM for control and Nav-Tsc2 mice with
851 corresponding p value and N. Small, medium and large diameter categorized defined in
852 Materials and Methods.

853 **Extended Data Figure 7-1.** RNA-seq analysis of FACS-sorted neurons from control; Rosa-GFP
854 and Nav-Tsc2; Rosa-GFP summarized in Figure 7. Red and blue text denotes upregulated and
855 downregulated genes, respectively, in Nav-Tsc2 DRG compared to control (adjusted $p<0.05$,
856 log2 fold change >0.5 or <-0.5). Black text denotes no change in expression. padj denotes
857 adjusted p value.

858

References

Abdel Samad, O., Liu, Y., Yang, F. C., Kramer, I., Arber, S., & Ma, Q. (2010). Characterization of two Runx1-dependent nociceptor differentiation programs necessary for inflammatory versus neuropathic pain. *Mol Pain, 6*, 45. doi:10.1186/1744-8069-6-45

Abe, N., Borson, S. H., Gambello, M. J., Wang, F., & Cavalli, V. (2010). Mammalian target of rapamycin (mTOR) activation increases axonal growth capacity of injured peripheral nerves. *J Biol Chem, 285*(36), 28034-28043. doi:10.1074/jbc.M110.125336

Agarwal, N., Offermanns, S., & Kuner, R. (2004). Conditional gene deletion in primary nociceptive neurons of trigeminal ganglia and dorsal root ganglia. *Genesis, 38*(3), 122-129. doi:10.1002/gene.20010

Asante, C. O., Wallace, V. C., & Dickenson, A. H. (2010). Mammalian target of rapamycin signaling in the spinal cord is required for neuronal plasticity and behavioral hypersensitivity associated with neuropathy in the rat. *J Pain, 11*(12), 1356-1367. doi:10.1016/j.jpain.2010.03.013

Beirowski, B., Wong, K. M., Babetto, E., & Milbrandt, J. (2017). mTORC1 promotes proliferation of immature Schwann cells and myelin growth of differentiated Schwann cells. *Proc Natl Acad Sci U S A, 114*(21), E4261-E4270. doi:10.1073/pnas.1620761114

Bennett, D. L., Michael, G. J., Ramachandran, N., Munson, J. B., Averill, S., Yan, Q., . . . Priestley, J. V. (1998). A distinct subgroup of small DRG cells express GDNF receptor components and GDNF is protective for these neurons after nerve injury. *Journal of Neuroscience, 18*(8), 3059-3072.

Brenner, D. S., Golden, J. P., & Gereau, R. W. t. (2012). A novel behavioral assay for measuring cold sensation in mice. *PLoS One, 7*(6), e39765. doi:10.1371/journal.pone.0039765

883 Budde, K., Becker, T., Arns, W., Sommerer, C., Reinke, P., Eisenberger, U., . . .
884 Investigators, Z. S. (2011). Everolimus-based, calcineurin-inhibitor-free regimen in
885 recipients of de-novo kidney transplants: an open-label, randomised, controlled trial.
886 *Lancet, 377*(9768), 837-847. doi:10.1016/S0140-6736(10)62318-5
887 Cavanaugh, D. J., Lee, H., Lo, L., Shields, S. D., Zylka, M. J., Basbaum, A. I., &
888 Anderson, D. J. (2009). Distinct subsets of unmyelinated primary sensory fibers mediate
889 behavioral responses to noxious thermal and mechanical stimuli. *Proc Natl Acad Sci U*
890 *S A, 106*(22), 9075-9080. doi:10.1073/pnas.0901507106
891 Cevikbas, F., Wang, X., Akiyama, T., Kempkes, C., Savinko, T., Antal, A., . . . Steinhoff,
892 M. (2014). A sensory neuron-expressed IL-31 receptor mediates T helper cell-
893 dependent itch: Involvement of TRPV1 and TRPA1. *J Allergy Clin Immunol, 133*(2),
894 448-460. doi:10.1016/j.jaci.2013.10.048
895 Chaplan, S. R., Bach, F. W., Pogrel, J. W., Chung, J. M., & Yaksh, T. L. (1994).
896 Quantitative assessment of tactile allodynia in the rat paw. *J Neurosci Methods, 53*(1),
897 55-63.
898 Chen, C. L., Broom, D. C., Liu, Y., de Nooij, J. C., Li, Z., Cen, C., . . . Ma, Q. (2006).
899 Runx1 determines nociceptive sensory neuron phenotype and is required for thermal
900 and neuropathic pain. *Neuron, 49*(3), 365-377. doi:10.1016/j.neuron.2005.10.036
901 Chiu, I. M., Barrett, L. B., Williams, E. K., Strochlic, D. E., Lee, S., Weyer, A. D., . . .
902 Woolf, C. J. (2014). Transcriptional profiling at whole population and single cell levels
903 reveals somatosensory neuron molecular diversity. *Elife, 3*. doi:10.7554/eLife.04660
904 Cho, Y., Di Liberto, V., Carlin, D., Abe, N., Li, K. H., Burlingame, A. L., . . . Cavalli, V.
905 (2014). Syntaxin13 expression is regulated by mammalian target of rapamycin (mTOR)

in injured neurons to promote axon regeneration. *J Biol Chem, 289*(22), 15820-15832. doi:10.1074/jbc.M113.536607

Ercan, E., Han, J. M., Di Nardo, A., Winden, K., Han, M. J., Hoyo, L., . . . Sahin, M. (2017). Neuronal CTGF/CCN2 negatively regulates myelination in a mouse model of tuberous sclerosis complex. *J Exp Med, 214*(3), 681-697. doi:10.1084/jem.20160446

Feltri, M. L., Poitelon, Y., & Previtali, S. C. (2016). How Schwann Cells Sort Axons: New Concepts. *Neuroscientist, 22*(3), 252-265. doi:10.1177/1073858415572361

Ferrari, L. F., Bogen, O., Chu, C., & Levine, J. D. (2013). Peripheral administration of translation inhibitors reverses increased hyperalgesia in a model of chronic pain in the rat. *J Pain, 14*(7), 731-738. doi:10.1016/j.jpain.2013.01.779

Fingar, D. C., Salama, S., Tsou, C., Harlow, E., & Blenis, J. (2002). Mammalian cell size is controlled by mTOR and its downstream targets S6K1 and 4EBP1/eIF4E. *Genes Dev, 16*(12), 1472-1487. doi:10.1101/gad.995802

Gallaher, Z. R., & Steward, O. (2018). Modest enhancement of sensory axon regeneration in the sciatic nerve with conditional co-deletion of PTEN and SOCS3 in the dorsal root ganglia of adult mice. *Exp Neurol, 303*, 120-133. doi:10.1016/j.expneurol.2018.02.012

Geranton, S. M., Jimenez-Diaz, L., Torsney, C., Tochiki, K. K., Stuart, S. A., Leith, J. L., . . . Hunt, S. P. (2009). A rapamycin-sensitive signaling pathway is essential for the full expression of persistent pain states. *Journal of Neuroscience, 29*(47), 15017-15027. doi:10.1523/JNEUROSCI.3451-09.2009

Gomez-Sanchez, J. A., Pilch, K. S., van der Lans, M., Fazal, S. V., Benito, C., Wagstaff, L. J., . . . Jessen, K. R. (2017). After Nerve Injury, Lineage Tracing Shows That Myelin

and Remak Schwann Cells Elongate Extensively and Branch to Form Repair Schwann Cells, Which Shorten Radically on Remyelination. *Journal of Neuroscience, 37*(37), 9086-9099. doi:10.1523/JNEUROSCI.1453-17.2017

Hasegawa, H., Abbott, S., Han, B. X., Qi, Y., & Wang, F. (2007). Analyzing somatosensory axon projections with the sensory neuron-specific Advillin gene. *Journal of Neuroscience, 27*(52), 14404-14414. doi:10.1523/JNEUROSCI.4908-07.2007

Hernandez, O., Way, S., McKenna, J., 3rd, & Gambello, M. J. (2007). Generation of a conditional disruption of the Tsc2 gene. *Genesis, 45*(2), 101-106. doi:10.1002/dvg.20271

Isotani, S., Hara, K., Tokunaga, C., Inoue, H., Avruch, J., & Yonezawa, K. (1999). Immunopurified mammalian target of rapamycin phosphorylates and activates p70 S6 kinase alpha in vitro. *J Biol Chem, 274*(48), 34493-34498.

Jiang, Z., Wu, S., Wu, X., Zhong, J., Lv, A., Jiao, J., & Chen, Z. (2016). Blocking mammalian target of rapamycin alleviates bone cancer pain and morphine tolerance via micro-opioid receptor. *Int J Cancer, 138*(8), 2013-2020. doi:10.1002/ijc.29927

Jimenez-Diaz, L., Geranton, S. M., Passmore, G. M., Leith, J. L., Fisher, A. S., Berliocchi, L., . . . Hunt, S. P. (2008). Local translation in primary afferent fibers regulates nociception. *PLoS One, 3*(4), e1961. doi:10.1371/journal.pone.0001961

Jones, E. A., Jang, S. W., Mager, G. M., Chang, L. W., Srinivasan, R., Gokey, N. G., . . . Svaren, J. (2007). Interactions of Sox10 and Egr2 in myelin gene regulation. *Neuron Glia Biol, 3*(4), 377-387. doi:10.1017/S1740925X08000173

950 Khoutorsky, A., Bonin, R. P., Sorge, R. E., Gkogkas, C. G., Pawlowski, S. A.,
951 Jafarnejad, S. M., . . . Sonenberg, N. (2015). Translational control of nociception via 4E-
952 binding protein 1. *Elife, 4*. doi:10.7554/eLife.12002
953 Khoutorsky, A., & Price, T. J. (2018). Translational Control Mechanisms in Persistent
954 Pain. *Trends Neurosci, 41*(2), 100-114. doi:10.1016/j.tins.2017.11.006
955 Kwon, M., Han, J., Kim, U. J., Cha, M., Um, S. W., Bai, S. J., . . . Lee, B. H. (2017).
956 Inhibition of Mammalian Target of Rapamycin (mTOR) Signaling in the Insular Cortex
957 Alleviates Neuropathic Pain after Peripheral Nerve Injury. *Front Mol Neurosci, 10*, 79.
958 doi:10.3389/fnmol.2017.00079
959 Liang, L., Tao, B., Fan, L., Yaster, M., Zhang, Y., & Tao, Y. X. (2013). mTOR and its
960 downstream pathway are activated in the dorsal root ganglion and spinal cord after
961 peripheral inflammation, but not after nerve injury. *Brain Res, 1513*, 17-25.
962 doi:10.1016/j.brainres.2013.04.003
963 Liu, K., Lu, Y., Lee, J. K., Samara, R., Willenberg, R., Sears-Kraxberger, I., . . . He, Z.
964 (2010). PTEN deletion enhances the regenerative ability of adult corticospinal neurons.
965 *Nat Neurosci, 13*(9), 1075-1081. doi:10.1038/nn.2603
966 Liu, Q., Tang, Z., Surdenikova, L., Kim, S., Patel, K. N., Kim, A., . . . Dong, X. (2009).
967 Sensory neuron-specific GPCR Mrgprs are itch receptors mediating chloroquine-
968 induced pruritus. *Cell, 139*(7), 1353-1365. doi:10.1016/j.cell.2009.11.034
969 Lutz, B. M., Nia, S., Xiong, M., Tao, Y. X., & Bekker, A. (2015). mTOR, a new potential
970 target for chronic pain and opioid-induced tolerance and hyperalgesia. *Mol Pain, 11*, 32.
971 doi:10.1186/s12990-015-0030-5

Madisen, L., Zwingman, T. A., Sunkin, S. M., Oh, S. W., Zariwala, H. A., Gu, H., . . . Zeng, H. (2010). A robust and high-throughput Cre reporting and characterization system for the whole mouse brain. *Nat Neurosci, 13*(1), 133-140. doi:10.1038/nn.2467

McCormack, F. X., Inoue, Y., Moss, J., Singer, L. G., Strange, C., Nakata, K., . . . Group, M. T. (2011). Efficacy and safety of sirolimus in lymphangioleiomyomatosis. *N Engl J Med, 364*(17), 1595-1606. doi:10.1056/NEJMoa1100391

McCoy, E. S., Taylor-Blake, B., Street, S. E., Pribisko, A. L., Zheng, J., & Zylka, M. J. (2013). Peptidergic CGRPalpha primary sensory neurons encode heat and itch and tonically suppress sensitivity to cold. *Neuron, 78*(1), 138-151. doi:10.1016/j.neuron.2013.01.030

Meikle, L., Talos, D. M., Onda, H., Pollizzi, K., Rotenberg, A., Sahin, M., . . . Kwiatkowski, D. J. (2007). A mouse model of tuberous sclerosis: neuronal loss of Tsc1 causes dysplastic and ectopic neurons, reduced myelination, seizure activity, and limited survival. *Journal of Neuroscience, 27*(21), 5546-5558. doi:10.1523/JNEUROSCI.5540-06.2007

Melemedjian, O. K., Asiedu, M. N., Tillu, D. V., Peebles, K. A., Yan, J., Ertz, N., . . . Price, T. J. (2010). IL-6-and NGF-Induced Rapid Control of Protein Synthesis and Nociceptive Plasticity via Convergent Signaling to the eIF4F Complex. *Journal of Neuroscience, 30*(45), 15113-15123. doi:10.1523/Jneurosci.3947-10.2010

Melemedjian, O. K., Khoutorsky, A., Sorge, R. E., Yan, J., Asiedu, M. N., Valdez, A., . . . Price, T. J. (2013). mTORC1 inhibition induces pain via IRS-1-dependent feedback activation of ERK. *Pain, 154*(7), 1080-1091. doi:10.1016/j.pain.2013.03.021

994 Mishra, S. K., & Hoon, M. A. (2013). The cells and circuitry for itch responses in mice.
995 *Science, 340*(6135), 968-971. doi:10.1126/science.1233765
996 Molliver, D. C., Wright, D. E., Leitner, M. L., Parsadanian, A. S., Doster, K., Wen, D., . . .
997 Snider, W. D. (1997). IB4-binding DRG neurons switch from NGF to GDNF dependence
998 in early postnatal life. *Neuron, 19*(4), 849-861.
999 Murinson, B. B., Hoffman, P. N., Banihashemi, M. R., Meyer, R. A., & Griffin, J. W.
1000 (2005). C-fiber (Remak) bundles contain both isolectin B4-binding and calcitonin gene-
1001 related peptide-positive axons. *J Comp Neurol, 484*(4), 392-402. doi:10.1002/cne.20506
1002 Nicks, J., Lee, S., Harris, A., Falk, D. J., Todd, A. G., Arredondo, K., . . . Notterpek, L.
1003 (2014). Rapamycin improves peripheral nerve myelination while it fails to benefit
1004 neuromuscular performance in neuropathic mice. *Neurobiol Dis, 70*, 224-236.
1005 doi:10.1016/j.nbd.2014.06.023
1006 Nie, D., Di Nardo, A., Han, J. M., Baharanyi, H., Kramvis, I., Huynh, T., . . . Sahin, M.
1007 (2010). Tsc2-Rheb signaling regulates EphA-mediated axon guidance. *Nat Neurosci,*
1008 *13*(2), 163-172. doi:10.1038/nn.2477
1009 Obara, I., Geranton, S. M., & Hunt, S. P. (2012). Axonal protein synthesis: a potential
1010 target for pain relief? *Curr Opin Pharmacol, 12*(1), 42-48.
1011 doi:10.1016/j.coph.2011.10.005
1012 Obara, I., & Hunt, S. P. (2014). Axonal protein synthesis and the regulation of primary
1013 afferent function. *Dev Neurobiol, 74*(3), 269-278. doi:10.1002/dneu.22133
1014 Obara, I., Medrano, M. C., Signoret-Genest, J., Jimenez-Diaz, L., Geranton, S. M., &
1015 Hunt, S. P. (2015). Inhibition of the mammalian target of rapamycin complex 1 signaling

1016 pathway reduces itch behaviour in mice. *Pain, 156*(8), 1519-1529.
1017 doi:10.1097/j.pain.0000000000000197
1018 Obara, I., Tochiki, K. K., Geranton, S. M., Carr, F. B., Lumb, B. M., Liu, Q., & Hunt, S. P.
1019 (2011). Systemic inhibition of the mammalian target of rapamycin (mTOR) pathway
1020 reduces neuropathic pain in mice. *Pain, 152*(11), 2582-2595.
1021 doi:10.1016/j.pain.2011.07.025
1022 Onda, H., Lueck, A., Marks, P. W., Warren, H. B., & Kwiatkowski, D. J. (1999). Tsc2(+/-)
1023 mice develop tumors in multiple sites that express gelsolin and are influenced by
1024 genetic background. *J Clin Invest, 104*(6), 687-695. doi:10.1172/JCI7319
1025 Park, K. K., Liu, K., Hu, Y., Smith, P. D., Wang, C., Cai, B., . . . He, Z. (2008). Promoting
1026 axon regeneration in the adult CNS by modulation of the PTEN/mTOR pathway.
1027 *Science, 322*(5903), 963-966. doi:10.1126/science.1161566
1028 Price, T. J., Rashid, M. H., Millecamps, M., Sanoja, R., Entrena, J. M., & Cervero, F.
1029 (2007). Decreased nociceptive sensitization in mice lacking the fragile X mental
1030 retardation protein: role of mGluR1/5 and mTOR. *Journal of Neuroscience, 27*(51),
1031 13958-13967. doi:10.1523/JNEUROSCI.4383-07.2007
1032 Ridler, K., Bullmore, E. T., De Vries, P. J., Suckling, J., Barker, G. J., Meara, S. J., . . .
1033 Bolton, P. F. (2001). Widespread anatomical abnormalities of grey and white matter
1034 structure in tuberous sclerosis. *Psychol Med, 31*(8), 1437-1446.
1035 Saxton, R. A., & Sabatini, D. M. (2017). mTOR Signaling in Growth, Metabolism, and
1036 Disease. *Cell, 168*(6), 960-976. doi:10.1016/j.cell.2017.02.004

1037 Shields, S. D., Ahn, H. S., Yang, Y., Han, C., Seal, R. P., Wood, J. N., . . . Dib-Hajj, S.
1038 D. (2012). Nav1.8 expression is not restricted to nociceptors in mouse peripheral
1039 nervous system. *Pain, 153*(10), 2017-2030. doi:10.1016/j.pain.2012.04.022
1040 Svaren, J., & Meijer, D. (2008). The molecular machinery of myelin gene transcription in
1041 Schwann cells. *Glia, 56*(14), 1541-1551. doi:10.1002/glia.20767
1042 Tavazoie, S. F., Alvarez, V. A., Ridenour, D. A., Kwiatkowski, D. J., & Sabatini, B. L.
1043 (2005). Regulation of neuronal morphology and function by the tumor suppressors Tsc1
1044 and Tsc2. *Nat Neurosci, 8*(12), 1727-1734. doi:10.1038/nn1566
1045 Terenzio, M., Koley, S., Samra, N., Rishal, I., Zhao, Q., Sahoo, P. K., . . . Fainzilber, M.
1046 (2018). Locally translated mTOR controls axonal local translation in nerve injury.
1047 *Science, 359*(6382), 1416-1421. doi:10.1126/science.aan1053
1048 Usoskin, D., Furlan, A., Islam, S., Abdo, H., Lonnerberg, P., Lou, D., . . . Ernfors, P.
1049 (2015). Unbiased classification of sensory neuron types by large-scale single-cell RNA
1050 sequencing. *Nat Neurosci, 18*(1), 145-153. doi:10.1038/nn.3881
1051 Wang, X., Spandidos, A., Wang, H., & Seed, B. (2012). PrimerBank: a PCR primer
1052 database for quantitative gene expression analysis, 2012 update. *Nucleic Acids Res,*
1053 *40*(Database issue), D1144-1149. doi:10.1093/nar/gkr1013
1054 Xu, J. T., Zhao, X., Yaster, M., & Tao, Y. X. (2010). Expression and distribution of
1055 mTOR, p70S6K, 4E-BP1, and their phosphorylated counterparts in rat dorsal root
1056 ganglion and spinal cord dorsal horn. *Brain Res, 1336*, 46-57.
1057 doi:10.1016/j.brainres.2010.04.010
1058 Yang, F. C., Tan, T., Huang, T., Christianson, J., Samad, O. A., Liu, Y., . . . Ma, Q.
1059 (2013). Genetic control of the segregation of pain-related sensory neurons innervating

1060 the cutaneous versus deep tissues. *Cell Rep,* *5*(5), 1353-1364.
1061 doi:10.1016/j.celrep.2013.11.005
1062 Zylka, M. J., Sowa, N. A., Taylor-Blake, B., Twomey, M. A., Herrala, A., Voikar, V., &
1063 Vihko, P. (2008). Prostatic acid phosphatase is an ectonucleotidase and suppresses
1064 pain by generating adenosine. *Neuron,* *60*(1), 111-122.
1065 doi:10.1016/j.neuron.2008.08.024

1066

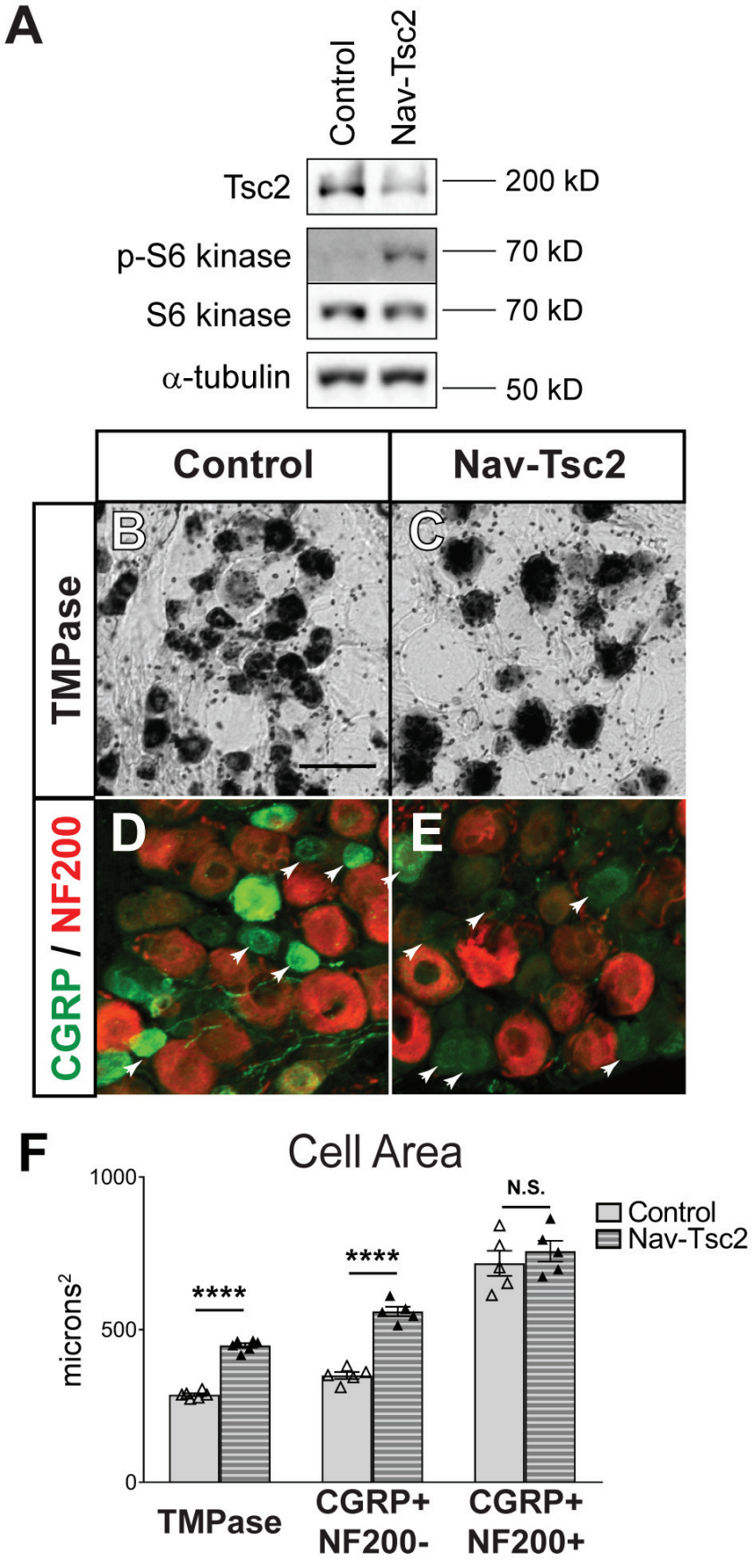

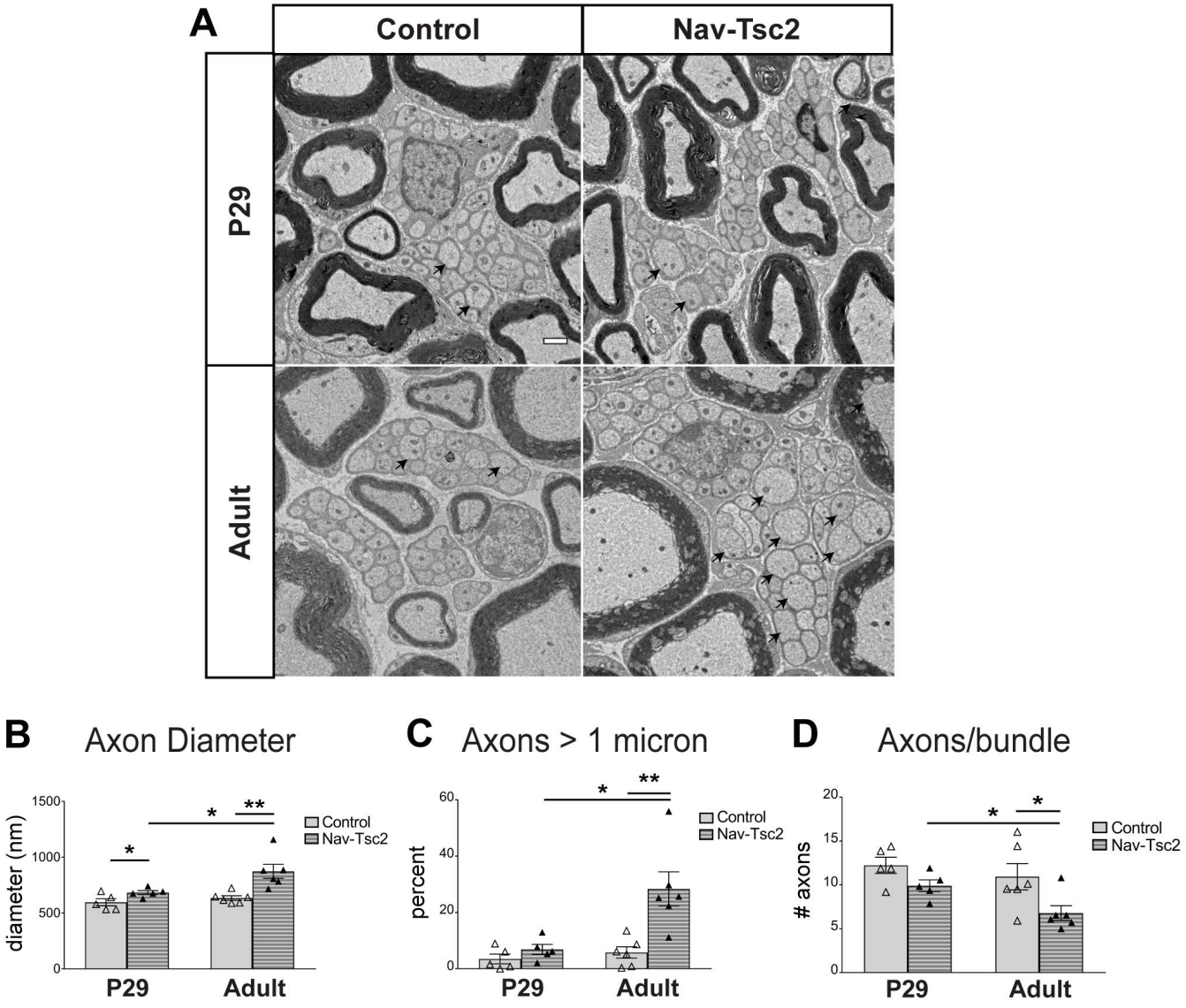

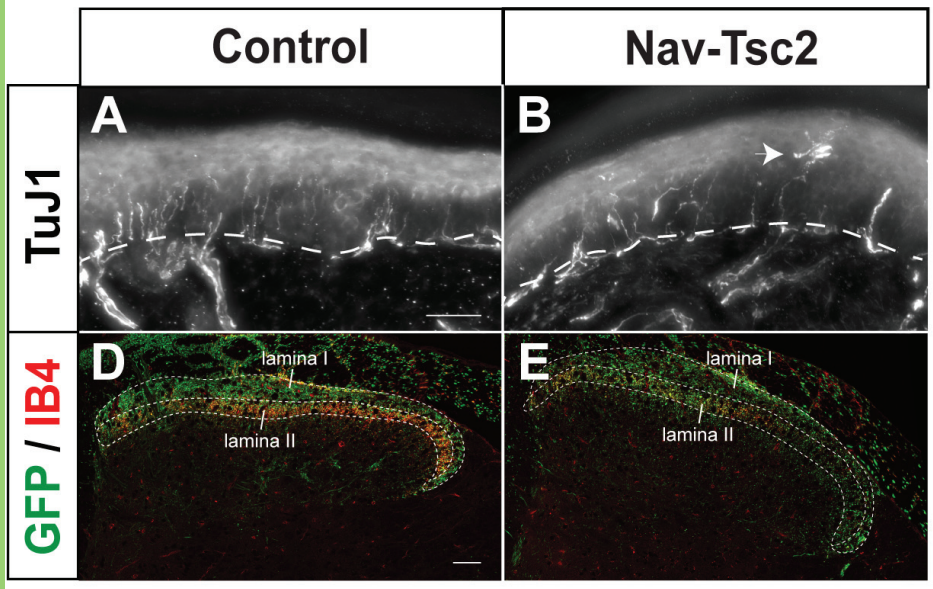

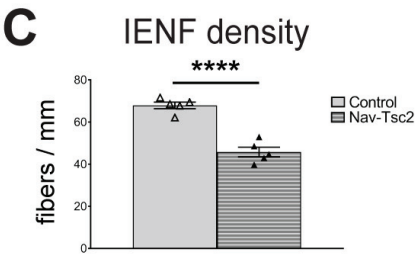

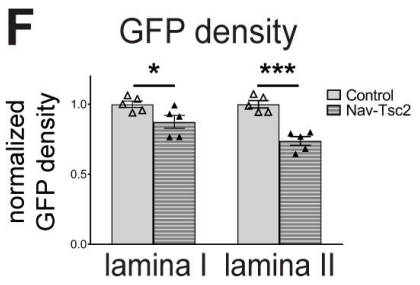

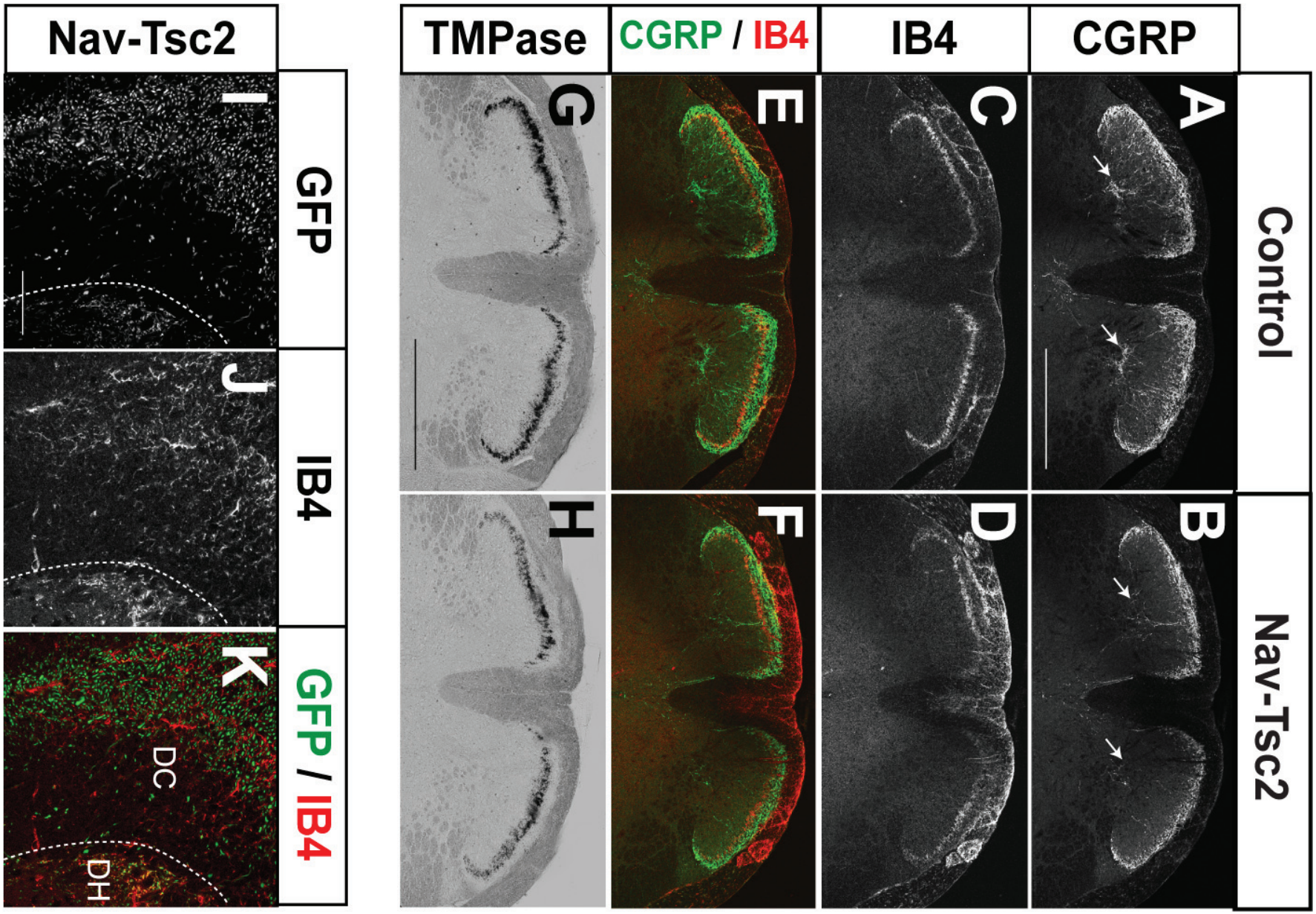

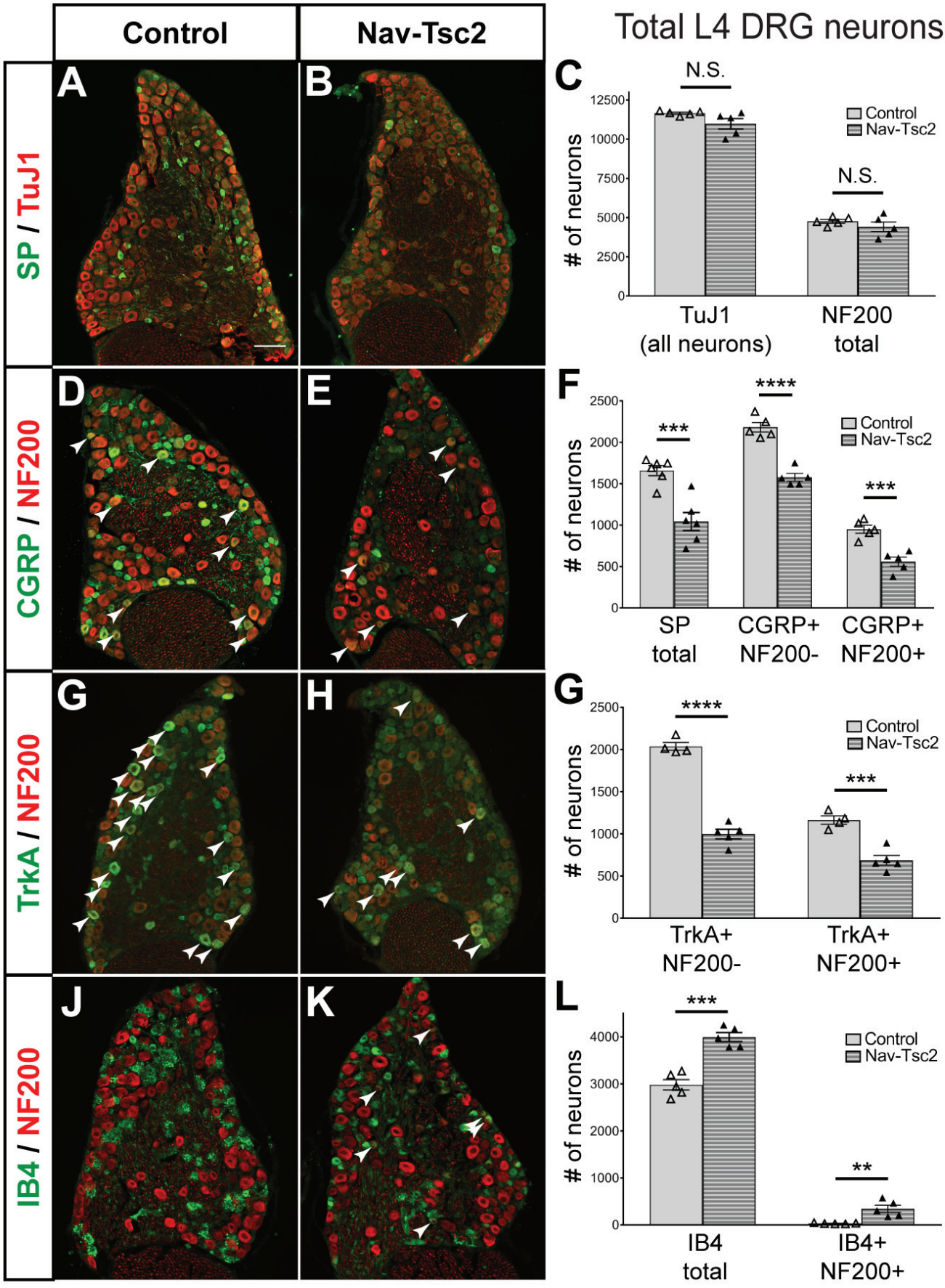

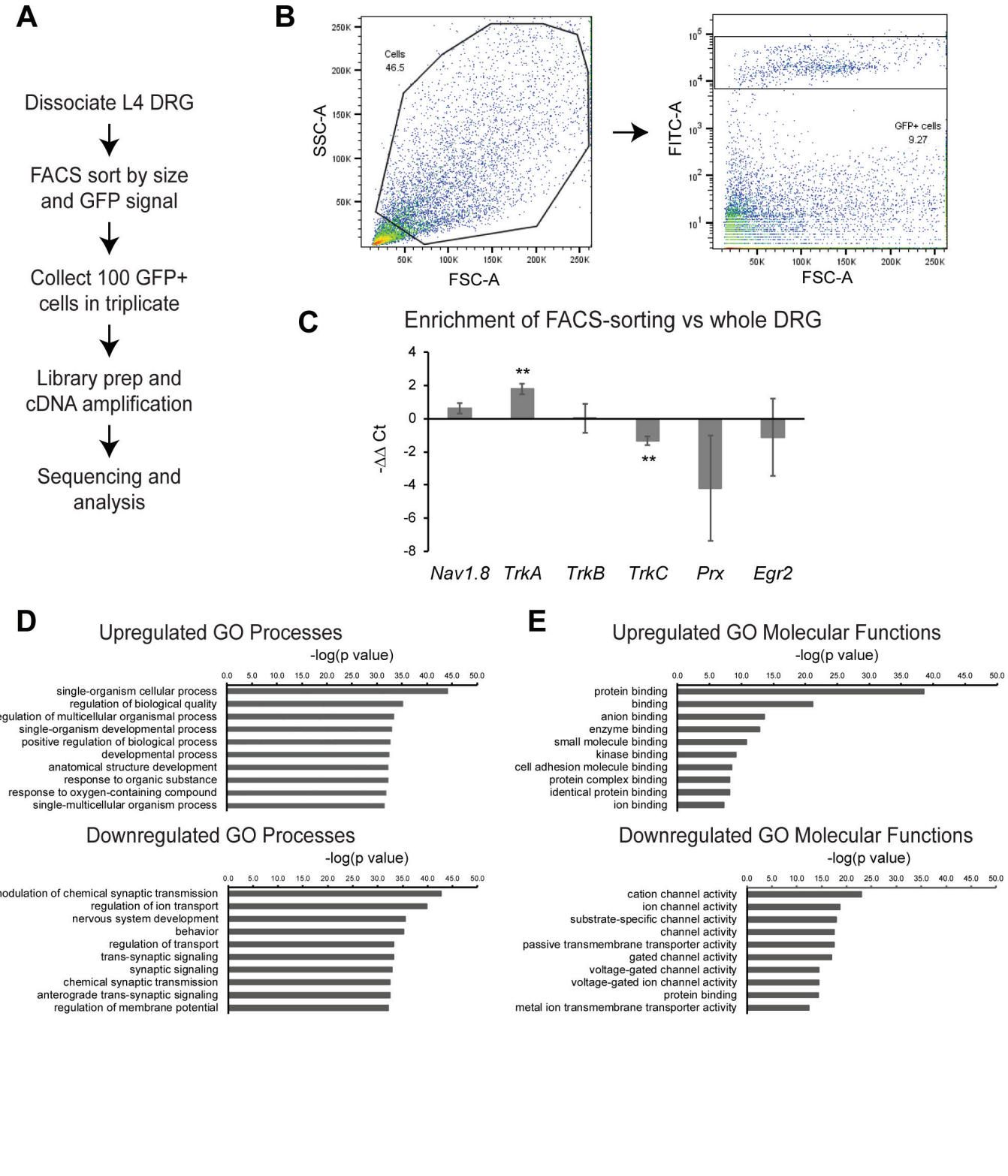

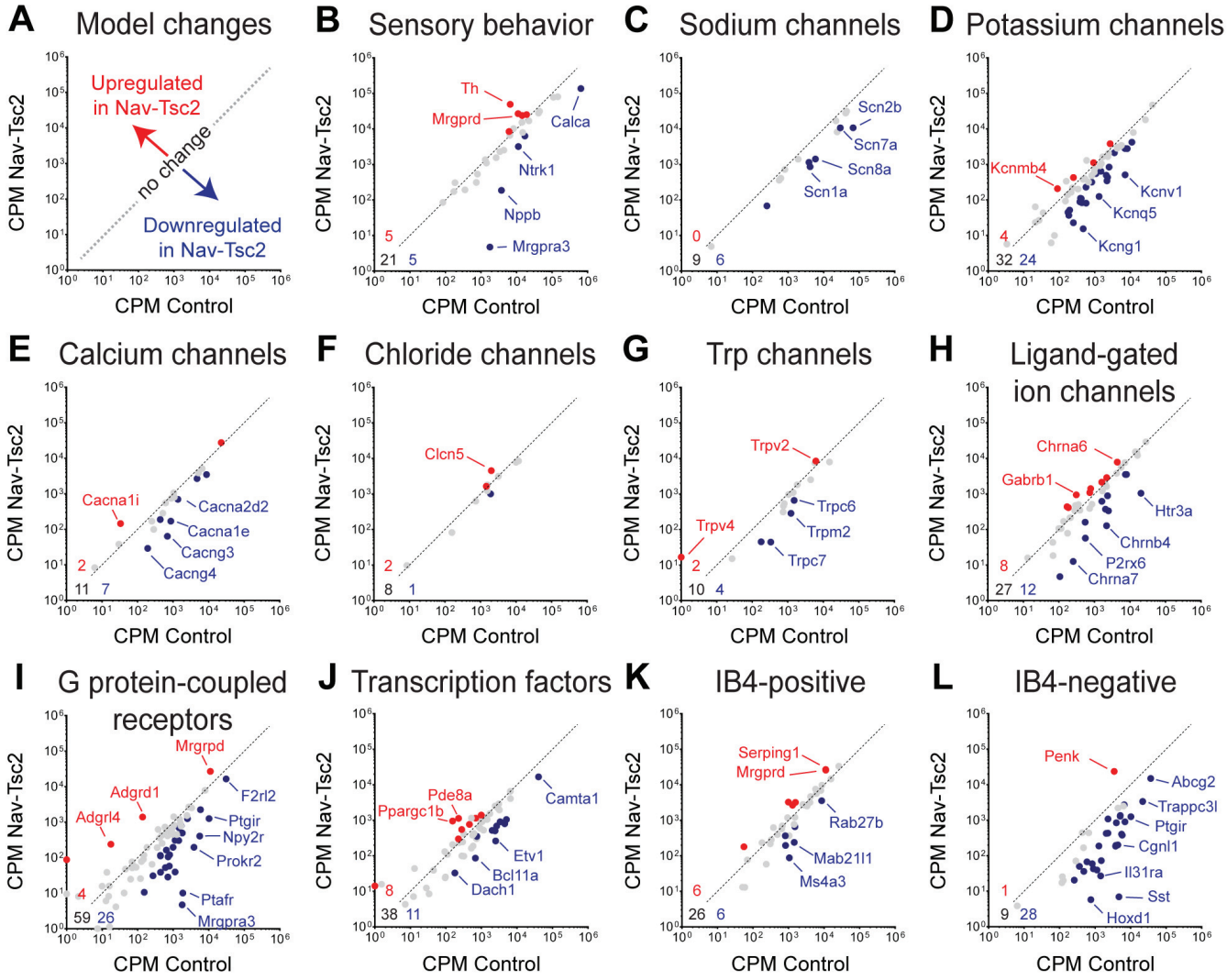

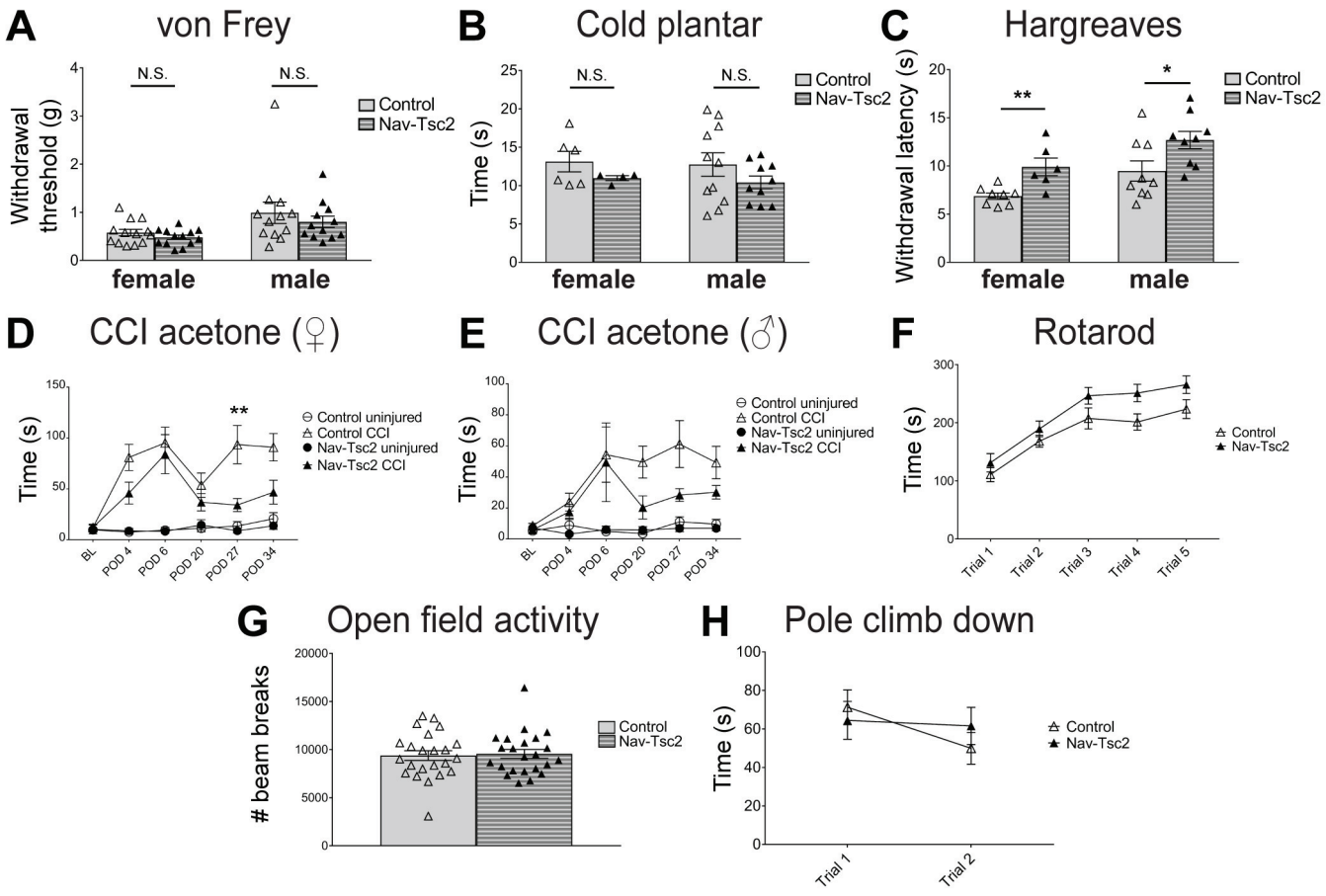

Table 1.

Gene name	Forward primer (5'-3')	Reverse primer (5'-3')
Ntrk1 / TrkA	GCCTAACCATCGTGAAGAGTG	CCAACGCATTGGAGGACAGAT
Scn10a / Nav1.8	TCCGTGGGAACTACCAACTTC	GCTCGCCATAGAACCTGGG
Ntrk2 / TrkB	CTGGGGCTTATGCCTGCTG	AGGCTCAGTACACCAAATCCTA
Ntrk3 / TrkC	CCGCATCCCAGTCATTGAGAA	TGACCTTGGGTAAGACACATCC
Periaxin	CTCAGCTTGCAAGAAGGGGA	CGTACCAGCTTGGCCACTTT
Egr2 / Krox20	GGCTCAGTTCAACCCCTCTC	GCGCAAAAGTCCTGTGTGTT

Table 2.

Figure	Statistical test	N	Statistical significance
1E Cell area	unpaied t test, two-tailed	TMPase: N=6 CGRP: N=5	TMPase: P<0.0001 CGRP+,NF200-: P<0.0001 CGRP+,NF200+: P=0.4803
Table 3 Cell distribution	unpaied t test, two-tailed	N=5-6	See Table 3
2B Axon diameter	unpaied t test, two-tailed	adult: N=6 P29: N=5	Adult control vs adult Nav-Tsc2: P=0.0047 P29 control vs P29 Nav-Tsc2: P=0.0442 Adult control vs P29 control: P=0.318 Adult Nav-Tsc2 vs P29 Nav-Tsc2: P=0.0258
2C Axons >1 micron	unpaied t test, two-tailed	adult: N=6 P29: N=5	Adult control vs adult Nav-Tsc2: P=0.0055 P29 control vs P29 Nav-Tsc2: P=0.2076 Adult control vs P29 control: P=0.4211 Adult Nav-Tsc2 vs P29 Nav-Tsc2: P=0.0125
2D Axons/bundle	unpaied t test, two-tailed	adult: N=6 P29: N=5	Adult control vs adult Nav-Tsc2: P=0.0371 P29 control vs P29 Nav-Tsc2: P=0.0747 Adult control vs P29 control: P=0.5018 Adult Nav-Tsc2 vs P29 Nav-Tsc2: P=0.0202
3C Skin innervation	unpaied t test, two-tailed	N=5	TuJ1: P<0.0001
3F GFP density	unpaied t test, two-tailed	N=5	Lamina I: P=0.0403 Lamina II: P=0.0002
5C,F,G,L DRG neuron counting	unpaied t test, two-tailed	N=5 SP: N=6	Total neurons: P=0.081 NF200 total: P=0.314 SP total: P=0.0006 CGRP+,NF200-: P<0.0001 CGRP+,NF200+: P=0.0007 TrkA+,NF200-: P<0.0001 TrkA+,NF200+: P=0.0005 IB4 total: P=0.0001 IB4+,NF200+: P=0.0037
6C qPCR of FACS-sorting	unpaied t test, two-tailed	N=4 whole DRG N=3 FACS-sorted samples	Nav1.8: P=0.0613 TrkA: P=0.0015 TrkB: P=0.9758 TrkC: P=0.0020 Prx: P=0.1784 Egr2: P=0.5834
8A von Frey	unpaied t test, two-tailed	female: N=13 male: N=12	female: P=0.2513 male: P=0.462
8B	unpaied t test, two-tailed	female: N=6 control, 4	female: P=0.2390

		cKO	
Cold plantar		male: N=11 control, 10 cKO	male: P=0.2102
8C Hargreaves	unpaied t test, two-tailed	female: N=13 male: N=9	female: P=0.0046 male: P=0.0337
8D Female CCI	Two-way RM ANOVA	Control: N=9 Nav-Tsc2: N=8	Interaction: F (5, 75) = 1.82; P=0.1191 Time: F (5, 75) = 10.04; P<0.0001 Genotype: F (1, 15) = 9.032; P=0.0089
8D Female CCI	Sidak's multiple comparison test	Control: N=9 Nav-Tsc2: N=8	BL: adjusted P value >0.9999 POD 4: adjusted P value = 0.269 POD 6: adjusted P value = 0.9896 POD 20: adjusted P value = 0.9209 POD 27: adjusted P value = 0.0071 POD 34: adjusted P value = 0.0836
8E Male CCI	Two-way RM ANOVA	Control: N=11 Nav-Tsc2: N=10	Interaction: F (5, 75) = 0.7719; P=0.5723 Time: F (5, 95) = 4.873; P=0.0005 Genotype: F (1, 19) = 3.403; P=0.0807
8E Male CCI	Sidak's multiple comparison test	Control: N=11 Nav-Tsc2: N=10	BL: adjusted P value >0.9999 POD 4: adjusted P value = 0.9992 POD 6: adjusted P value = 0.9998 POD 20: adjusted P value = 0.3652 POD 27: adjusted P value = 0.236 POD 34: adjusted P value = 0.8045
8F Rotarod	Two-way RM ANOVA	Control: N=17 Nav-Tsc2: N=17	Interaction: F (4, 128) = 1.03; P=0.3946 Trial number: F (4, 128) = 60.26; P<0.0001 Genotype: F (1, 32) = 4.08; P=0.0518
8F Rotarod	Sidak's multiple comparison test	Control: N=17 Nav-Tsc2: N=17	Trial 1: adjusted P value = 0.8576 Trial 2: adjusted P value = 0.8396 Trial 3: adjusted P value = 0.2686 Trial 4: adjusted P value = 0.0812 Trial 5: adjusted P value = 0.1971
8G Open field activity	unpaied t test, two-tailed	Control: N=23 Nav-Tsc2: N=23	P=0.8027
8H Pole climb down	Two-way RM ANOVA	Control: N=23 Nav-Tsc2: N=22	Interaction: F (1, 43) = 2.62; P=0.1129 Trial number: F (1, 43) = 4.516; P=0.0394 Genotype: F (1, 43) = 0.04254; P=0.8376
8H Pole climb down	Sidak's multiple comparison test	Control: N=23 Nav-Tsc2: N=22	Trial 1: adjusted P value = 0.84 Trial 2: adjusted P value = 0.606

Table 3.

	small	medium	large
TMPase			
Control	67 ± 1.98 %	33 ± 1.98 %	0 ± 0 %
Nav-Tsc2	20.83 ± 1.68 %	73.83 ± 1.66 %	5.33 ± 1.31 %
p value (N)	< 0.0001 (6)	< 0.0001 (6)	0.0712 (6)
CGRP+, NF200-			
Control	41 ± 4.63 %	58.4 ± 4.5 %	0.6 ± 0.4 %
Nav-Tsc2	4.2 ± 1.88 %	77.8 ± 0.97 %	18 ± 2.35 %
p value (N)	< 0.0001 (5)	0.0003 (5)	0.001 (5)
CGRP+, NF200+			
Control	4.4 ± 0.75 %	46.8 ± 6.28 %	48.8 ± 6.22 %
Nav-Tsc2	2 ± 1.1 %	50.8 ± 3.83 %	47.2 ± 4.59 %
p value (N)	0.9736 (5)	0.893 (5)	0.9918 (5)